Dipartimento di Scienze

Dottorato di ricerca in biologia molecolare, cellulare e ambientale

XXX ciclo

Cross interaction between β-amyloid protein and adult neurogenesis during neurodegeneration: towards the identification of new therapeutical strategies for Alzheimer's disease.

Candidate
Chiara Scopa

Tutor
Prof.ssa Sandra Moreno

Co-tutor
Dr.ssa Raffaella Scardigli

Alla mia mamma,
che mi ha insegnato che
volere è potere
e
al mio papà,
che è il mio supereroe

Index

Summary

Adult neurogenesis is a multi-step process, which consists in the continuous generation of new neurons in the mammalian brain throughout adulthood. This process occurs in two brain regions of mammals, also called neurogenic niches, which are the subventricular zone (SVZ) of the lateral ventricle and the subgranular zone (SGZ) of the dentate gyrus of the hippocampus (DG-HP). The role of adult neurogenesis in neurodegenerative disorders, such as Alzheimer's disease (AD), is still under debate. Since the latter stages of AD are characterized by a massive loss of neurons, possible role of adult neurogenesis in the pathogenesis of this disease has been investigated. Indeed, the complete understanding of the role of neurogenesis in the pathology would exploit this physiological process as a possible therapy for Alzheimer's disease.

Alzheimer's disease (AD) animal models are still useful to study dynamic alteration of adult neurogenesis due to the fact that similar studies are no possible in humans. Conflicting observations have been reported regarding the level of neurogenesis in animal models of Alzheimer's disease. Furthermore, very little is known about differences in neurogenesis at the early stages of AD, before the onset of amyloid-plaque formation, one of the typical hallmarks of pathology progression. Indeed, there are increasing evidences that adult neurogenesis is under the influence of key molecules underlying Alzheimer's disease, such as the β-amyloid (Aβ) peptide. During disease progression, Aβ peptides assemble into various aggregation forms, ranging from dimers and oligomers to fibrils in amyloid plaques. However, the magnitude of amyloid plaque deposition in the brain correlates poorly with cognitive decline, and emerging evidence suggests that Aβ oligomers may be the major causes in this regard. However, it is still not clear how the pathophysiological environment in the AD brain, and in particular the different Aβ species, affect neural stem cell (NSC) biology and thus adult neurogenesis. Previous studies obtained controversial results, reporting that extracellular Aβ either decreases or increases proliferation, prevents or induces neurogenesis of NSCs. These discrepancies are likely due to the different animal and cellular models used

and, more important, the different Aβ species. Furthermore, none of these studies explored the role of intracellular Aβ generation and oligomerization, which is one of the earliest event in AD pathogenesis.

The aim of this thesis is to define how neurogenesis is regulated in Alzheimer's disease and if alterations in adult neurogenesis represent an early event in AD pathogenesis. I investigated neurogenesis in Tg2576 transgenic mice at an age (1-2 months) that is considered pre-symptomatic, in terms of Aβ accumulation and neurodegeneration. Moreover, since in these mice there is an overproduction Aβ oligomers (AβOs) in the nervous system, I investigated if naturally occurring Aβ oligomers, which represent the most neurotoxic species in AD, modulate NSCs biology, in view of possible cross-interaction between impaired neurogenesis and the amyloidogenic processing pathway. To better investigate this aim SVZ-and DG-derived aNSCs have been analyzed *in vitro* for their proliferation and differentiation potential in relationship with the biochemical profile of the different Aβ species. The ultimate goal of this research is to gain new insights into the molecular mechanisms that control adult neurogenesis in AD neurodegeneration and to develop new strategies to restore normal neurogenesis specifically in those brain regions where it is impaired.

By analyzing the proliferative and differentiative features of resident or SVZ-derived adult neural stem cells (aNSCs) I found that Tg2576 aNSCs proliferate significantly less, with respect to their control counterparts. Tg2576 neurospheres are enriched in DCX^+ neuroblasts, which failed to terminally differentiate, as demonstrated by the lower degree of maturation in terms of neurites arborization, and give rise to less GFAP+ astrocytes, with an aberrant morphology. These defects have been confirmed also *in vivo*, where a defective olfactory bulbs (OBs) neurogenesis is observed, as demonstrated by the reduced number of newborn interneurons $NueN^+$ and $CalR^+$ in Tg2576 OBs. I demonstrated that reduced proliferation and the differentiation impairment of Tg2576 progenitors *in vitro* are caused by endogenous oligomeric Aβ: indeed, both defects are rescued by the expression of a

conformation-specific intrabody, which selectively interferes with the early intracellular generation of Aβ oligomers. Noteworthy, the AβO-selective intrabody interference restores the pathological microtubule hyperstabilization of newly formed neurons, which is tau-mediated. Finally, lentiviral-mediated *in vivo* expression of the intrabody in Tg2576 SVZ rescues the olfactory bulbs neurogenesis, and restores SVZ-derived aNSCs proliferation and differentiation.

Early alterations in adult neurogenesis were also present in the other neurogenic niche of Tg2576 mice, the dentate gyrus of the hippocampus (DG-HP). Similarly to the SVZ-derived progenitors, hippocampal progenitors displayed high amount of intracellular Aβ oligomers and undergo neuronal and astrocytic differentiation impairment. Both defects were rescued by the AβOs intracellular targeting with an inducible scFvA13-KDEL intrabody. Comparable results were obtained in human neural progenitors (NPs) that stably expressed the ScFvA13 intrabody. Moreover, in order to analyze also the role of extracellular AβOs accumulation, that leads to Aβ plaques formation at the last stage of AD, Tg2576 aNSCs have been treated with the recombinant nanobody. In this way, I demonstrated that also extracellular AβOs played an important role in controlling both proliferation and differentiation of aNSCs. In fact, the extracellular administration of ScFvA13 nanobody to Tg2576 aNSCs significantly rescues their proliferative impairment as well as their neurogenic defects, in a dose-dependent manner. Strikingly, I demonstrated the efficacy of ScFvA13, both as intrabody and nanobody, in restoring AβOs-dependent proliferative and differentiative impairment also in human-AD NPs.

Altogether, my results demonstrate that impaired neurogenesis is an early event, occurring at a presymptomatic age prior to overt neurodegeneration and is caused by endogenous AβOs accumulation in the neurogenic niches. Notably, the intra- or extracellular interception of AβOs by scFvA13 antibody in aNSCs reestablishes proper neuronal and glial differentiation. This important finding demonstrates the potential efficacy of targeting AβOs in aNSCs as a therapeutic strategy to restrain neuronal degeneration in AD and validates the scFvA13

antibody as a new therapeutic tool, able to restore a functional neurogenesis.

Riassunto

La neurogenesi adulta è un processo a più fasi, che consiste nella generazione continua di nuovi neuroni nel cervello dei mammiferi durante l'età adulta. Questo processo avviene in due regioni del cervello dei mammiferi, chiamate anche nicchie neurogeniche, che sono la zona subventricolare (SVZ) del ventricolo laterale e la zona subgranulare (SGZ) del giro dentato dell'ippocampo (DG-HP). Poiché le ultime fasi del morbo di Alzheimer (AD), una malattia neurodegenerativa contraddistinta da progressiva perdita di memoria e deterioramento delle funzioni cognitive, sono caratterizzate da una massiccia perdita di neuroni, è stato studiato il possibile ruolo della neurogenesi adulta nella patogenesi di questa malattia. In effetti, la completa comprensione del ruolo della neurogenesi nella patologia potrebbe consentire di sfruttare questo processo fisiologico come possibile terapia per il morbo di Alzheimer. I modelli animali del morbo di Alzheimer (AD) sono ancora utili per studiare l'alterazione dinamica della neurogenesi adulta, in quanto studi simili non sono possibili negli esseri umani. Per quanto riguarda le alterazioni della neurogenesi adulta in modelli animali del morbo di Alzheimer sono stati riportati risultati contrastanti. Inoltre, si sa ancora molto poco sulle possibili alterazioni nella neurogenesi negli stadi iniziali dell'AD, ancor prima dell'inizio della formazione delle placche della proteina amiloide, uno dei tratti isto-patologici più caratteristici delle fasi avanzate della malattia. Infatti, numerose evidenze sperimentali hanno dimostrato che la neurogenesi adulta è sotto il controllo di molecole chiave coinvolte nella patogenesi della malattia di Alzheimer, quali il peptide β-amiloide (Aβ). Durante la progressione della malattia, i peptidi Aβ si aggregano in varie forme, che vanno dai dimeri, agli oligomeri, alle fibrille e infine alle placche amiloidi. Tuttavia, l'entità della deposizione delle placche amiloidi nel cervello non sempre correla con il declino cognitivo, e le recenti scoperte nel campo suggeriscono che gli Aβ oligomeri (AβOs) potrebbero essere la principale causa di tale declino. Tuttavia, non è ancora chiaro come l'ambiente fisiopatologico nel cervello AD, e in particolare le diverse specie di Aβ, influenzino la biologia delle cellule staminali neurali (NSCs) e quindi la neurogenesi adulta. Precedenti studi hanno ottenuto

risultati controversi, riportando che l'Aβ extracellulare diminuisce o aumenta la proliferazione, prevenendo o inducendo la neurogenesi delle NSCs. Queste differenze sono probabilmente dovute ai diversi modelli animali e cellulari utilizzati e, cosa più importante, alle diverse specie di Aβ analizzate. Inoltre, nessuno di questi studi ha esaminato il ruolo della generazione e dell'oligomerizzazione di Aβ intracellulare, che è uno dei primi eventi nella patogenesi dell'AD.

Lo scopo di questa tesi è definire come la neurogenesi è regolata nella malattia di Alzheimer e se le alterazioni nella neurogenesi adulta rappresentino un evento precoce nella patogenesi di questa patologia. Ho deciso di analizzare la neurogenesi in topi transgenici Tg2576 ad un'età (1-2 mesi) che è considerata pre-sintomatica, in termini di accumulo di Aβ e neurodegenerazione. Inoltre, poiché in questi topi è presente un eccesso di AβOs nel sistema nervoso, ho studiato se gli oligomeri di Aβ presenti in natura, che rappresentano la specie più neurotossica in AD, modulino la biologia delle NSCs, in vista di una possibile interazione molecolare tra neurogenesi alterata e la via amiloidogenica. Per indagare meglio tale obiettivo ho analizzato *in vitro* il potenziale di proliferazione e differenziamento delle aNSCs derivati da SVZ e DG-HP in relazione al loro profilo biochimico delle diverse specie Aβ. L'obiettivo finale di questa ricerca è di acquisire nuove conoscenze sui meccanismi molecolari che controllano la neurogenesi adulta nella neurodegenerazione AD per sviluppare in futuro nuove strategie terapeutiche volte a ripristinare la normale neurogenesi adulta, in particolare in quelle regioni del cervello in cui è compromessa.

Analizzando le caratteristiche proliferative e differenziative delle cellule staminali neurali adulte residenti e derivate dalla SVZ, abbiamo scoperto che le aNSCs dei topi Tg2576 proliferano significativamente meno, rispetto alla loro controparte WT. Inoltre, le neurosfere Tg2576 sono arricchite in neuroblasti DCX+, che però non riescono a differenziare completamente, come dimostrato dal basso grado di maturazione in termini di arborizzazione dei neuriti, e danno origine a meno astrociti GFAP+, con una morfologia aberrante. Questi difetti sono stati confermati anche *in vivo*, dove ho

potuto osservare una compromissione della neurogenesi dei bulbi olfattivi (OBs), come dimostrato dal ridotto numero di nuovi interneuroni NueN + e CalR + nei OBs dei topi Tg2576. In questo lavoro dimostro, inoltre, che sia la ridotta proliferazione che il mancato differenziamento terminale dei progenitori Tg2576 *in vitro* sono causate dall'accumulo intracellulare degli AβOs: infatti, entrambi i difetti sono recuperati dall'espressione di un anticorpo conformazionale e specifico, ScFvA13, che interferisce selettivamente con la generazione precoce ed intracellulare degli oligomeri di Aβ. In particolare, l'interferenza intracellulare e selettiva degli AβOs ripristina l'iper-stabilizzazione patologica dei microtubuli dei nuovi neuroni, che è mediata dalla proteina tau. Infine, l'espressione *in vivo* dell'anticorpo, ottenuta mediante un vettore lentivirale iniettato nella SVZ dei topi Tg2576, ripristina la neurogenesi dei bulbi olfattivi a livelli fisiologici, correggendo i difetti proliferativi e ristabilendo il corretto processo di differenziamento delle aNSCs derivate dall'SVZ.
L'alterazione precoce della neurogenesi adulta è presente anche nell'altra nicchia neurogenica dei topi Tg2576, il giro dentato dell'ippocampo (DG-HP). Analogamente ai progenitori derivati dalla SVZ, i progenitori dell'ippocampo presentano una quantità elevata di AβOs intracellulari insieme a difetti di differenziamento sia verso il lineage neuronale che gliale. Entrambi i difetti sono stati recuperati dal targeting intracellulare di AβOs tramite l'utilizzo di un vettore lentivirale inducibile, che esprime l'anticorpo scFvA13-KDEL. Risultati comparabili sono stati ottenuti nei progenitori neurali umani (NP), che esprimevano stabilmente l'anticorpo ScFvA13.
Inoltre, al fine di analizzare anche il ruolo dell'accumulo extracellulare di AβOs, responsabile della formazione di placche di Aβ che si verifica nell'ultimo stadio di AD, le aNSCs dei topi Tg2576 sono state trattate con l'anticorpo ricombinante. In questo modo, ho dimostrato che anche gli AβOs extracellulari giocano un ruolo importante nel controllare sia la proliferazione che il differenziamento delle cellule staminali neuronali adulte. Infatti, la somministrazione extracellulare dell'anticorpo ScFvA13 al terreno di coltura delle neurosfere Tg2576 determina un recupero significativo del loro deficit

proliferativo e dei loro difetti differenziativi, in modo dose-dipendente. Sorprendentemente, ho dimostrato l'efficacia di ScFvA13, sia come intrabody che come anticorpo, nel ripristinare il deficit proliferativo e differenziativo dipendente dagli Aβ oligomeri anche in precursori neuronali umani derivati da pazienti AD.

In conclusione, i miei risultati dimostrano che i difetti di neurogenesi adulta rappresentano un evento precoce, che si verifica ad un'età pre-sintomatica, prima della neurodegenerazione conclamata, e sono causati dall'accumulo di Aβ oligomeri presenti nelle nicchie neurogeniche. In particolare, l'interferenza intra- o extracellulare degli AβOs da parte dell'anticorpo scFvA13 nelle cellule staminali neuronali adulte ristabilisce il corretto differenziamento verso la linea neuronale e gliale. Questo importante risultato dimostra la potenziale efficacia del targeting degli AβOs come possibile strategia terapeutica per contrastare la degenerazione neuronale nell'AD e convalida l'anticorpo scFvA13 come nuovo strumento terapeutico, in grado di ripristinare una neurogenesi funzionale.

1.Introduction

1.1 Adult neurogenesis

Adult neurogenesis is the continuous generation of new neurons in the mammalian brain throughout adulthood. This process occurs in two brain regions of mammals, also called neurogenic niches, which are the subventricular zone (SVZ) of the lateral ventricle and the subgranular zone (SGZ) of the dentate gyrus (DG) in the hippocampus (Fig. 1).

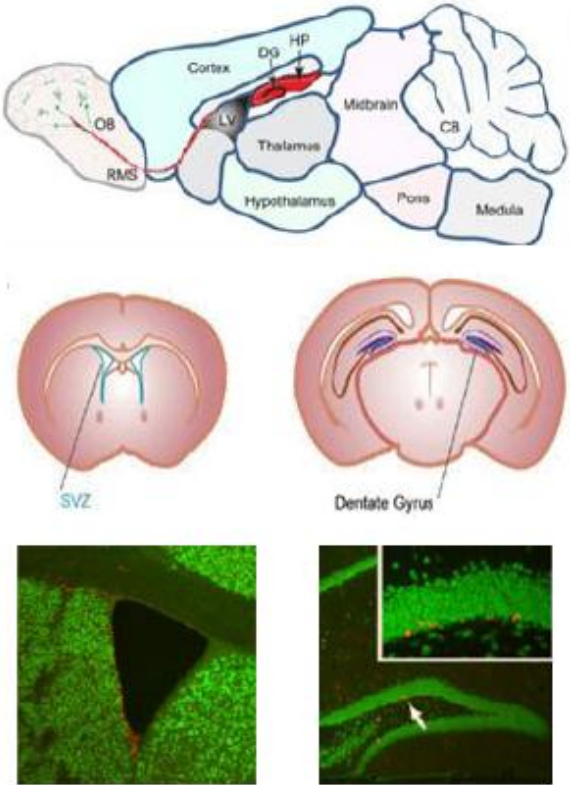

Figure 1. Anatomical view of adult NSCs niches in rodent brain in sagittal and coronal sections.

Neurogenesis is revealed by BrdU incorporation in SVZ and dentate gyrus (red, BrdU and green, NeuN), (Modified by Zhao *et al*., 2008; Vukonic *et al*., 2011; Ming and Song, 2011).

More recently, adult neurogenesis has been demonstrated also in the human striatum (Ernst *et al*., 2014). Neurons born in the adult SVZ, involving dopaminergic, GABAergic and glutamatergic interneurons, migrate through the rostral migratory stream (RSM) to populate several areas of the olfactory bulb, while neurons born in the adult SGZ migrate into the granule cell layer (GLC) of the dentate gyrus and become granule cells. Thus, adult neurogenesis is a multistep process involving: (*i*) proliferation of precursor cells, (*ii*) the acquisition of subtypes identity (fate determination); (*iii*) their differentiation and progressive maturation into fully differentiated neurons; (*iiii*) the functional integration of the newborn neurons into the exiting neural network (Zhao *et al*., 2008; Vukovic *et al*., 2011).
The two major neurogenic niches, SVZ and SGZ, have been extensively characterized both *in vivo* and *in vitro*, and throughout these studies new markers for specific type of progenitors populations have been identified, as described below.

1.2 The subgranular zone neurogenic niche

The subgranular zone niche is located adjacent to dentate hilus at the border of the GCL. Neural stem cells (NSCs) in the SGZ can be divided into several subtypes (Fig.2): (*i*) radial NSCs, typically quiescent cells, characterized morphologically by a single radial process and expressing the glial fibrillary acid protein (GFAP) and nestin; (*ii*) horizontal NSCs, expressing GFAP and nestin and morphologically characterized by short, horizontal processes. Both NSCs subtypes express the transcription factors Sox2, important for their “stemness”.

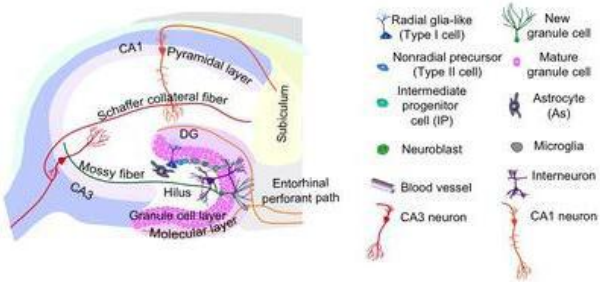

Figure 2. Schematic organization of subgranular zone in the dentate gyrus.
In this neurogenic niche multiple subtypes of NSCs coexist (Ming and Song, 2011).

One or both of these subtypes divide to give rise to transit-amplifying intermediate neuronal progenitors (INPs), which proliferate actively in the SGZ. Morphologically, the neuronal progenitors are small cells that tend to be present in clusters in the SGZ (Zhao *et al*., 2008; Hodge *et al*., 2012). Late-stage INPs are characterized by their expression of neuronal lineage markers, such as Doublecortin (Dcx) or marker of neuronal differentiation, such as NeuN (Fig.3).

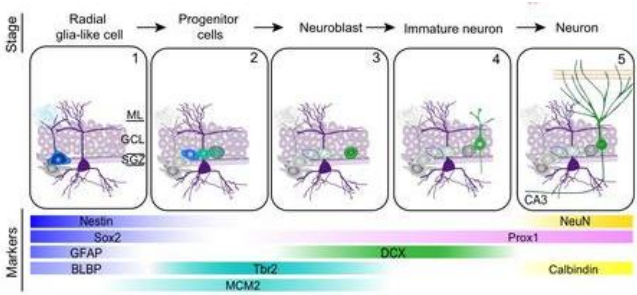

Figure 3. Schematic representation of neurogenesis process in adult hippocampus.
The progression from NSC to mature granule neuron is signaled by the expression of stage-specific cellular markers and transcription factors (Ming and Song, 2011).

1.3 The subventricular zone neurogenic niche

The SVZ niche is located adjacent to the ependymal cell layer of the lateral ventricles. The ependymal cells express the protein Noggin that may promote SVZ neurogenesis by antagonizing signaling of the bone morphogenetic proteins (BMPs), driving precursors through the neurogenic lineage.

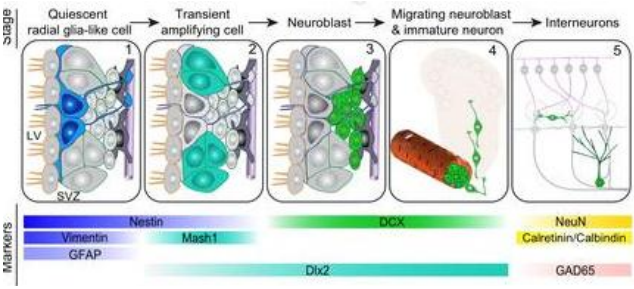

Figure 4. Schematic organization of SVZ in lateral ventricle.
Two types of glia-like cells have been proposed to be the local adult NSCs: type B cells and type C cells (Ming and song, 2011).

The adult SVZ consists of ependymal cells (type E cells) and primary NSCs (type B), that generate intermediate neuronal progenitors (INPs, type C) and finally immature neuroblasts (type A cells) (Fig.4).

NSCs typically express astrocyte-specific glutamate transporter (GLAST), GFAP, vimentin and nestin, while INPs are identified by the up-regulation of the transcription factors Asc11 and Dlx2 (Fig.5). At last, type A neuroblasts can be distinguished by the expression of Dcx and Tuj1 (β tubulin class III). These cells migrate through the rostral migratory stream (RMS) into the core of the olfactory bulb, where they contribute to long-neurogenesis in rodents (Zhao *et al*., 2008; Hodge *et al*., 2012), while in humans there is no evidence of the same contribution (Spalding *et al*., 2013).

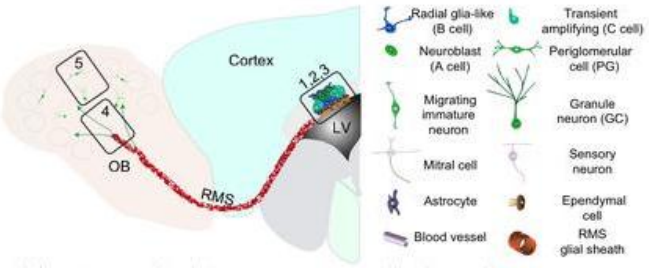

Figure 5. Schematic representation of neurogenesis process in SVZ niche.

The progression from NSC to mature granule neuron is signaled by expression of a stage-specific cellular markers and transcription factors (Ming and Song, 2011).

1.3.1 Striatal neurogenesis

Several studies have found neuroblasts that appear to exit the SVZ or rostral migratory stream and migrate through subcortical white matter tracts, suggesting that some neurons generated in the adult SVZ may incorporate into regions other than the olfactory bulb. Both the morphology of BrdU/DCX cells and their change in location with increasing survival time indicated that immature neurons or neuronal precursors in the SVZ do not all join the rostral migratory stream and may instead migrate into the striatum (Dayer *et al*., 2005). Employing transgenic mice expressing EGFP in GABAergic interneurons, Inta and colleagues identified additional migratory pathways in the early postnatal brain from the SVZ into numerous forebrain regions, including striatum (Inta *et al*., 2008). Later on, low levels of striatal neurogenesis have been reported in mice, rats, rabbits, and monkeys (Bergmann *et al*., 2015). In humans, SVZ neurogenesis poorly contributes to the generation of olfactory bulb interneurons (Bergamann *et al*., 2012). However, the presence of neuroblasts in the subventricular zone in adult humans, but very few migrating along the rostral migratory stream or giving rise to neurons in the olfactory bulbs, posed the question on the possible fate of these neuroblasts. (Ernst *et al*., 2014). The generation of neuroblasts in the subventricular zone, located adjacent to the

striatum, make it tempting to speculate that the new neurons in the adult human striatum might derive from the subventricular zone. Indeed, the generation of new striatal interneurons was formally demonstrated in humans by the detection of iododeoxyuridine (IdU)-positive neurons in postmortem tissue from cancer patients who had received IdU as a radiosensitizer (Ernst *et al*., 2014). Moreover, further indications of the extent of human striatal neurogenesis came from expression studies of immature neuron markers, such as Doublecortin (DCX), performed by mRNA in-situ hybridization experiments in post-mortem brains. Interestingly, DCX was found highly expressed in the striatum of human specimen. Despite these promising findings, currently we can only speculate about the potential functions of adult striatal neurogenesis in humans. The striatum has traditionally been primarily associated with motor functions, and more recently, to procedural learning and memory, as well as with cognitive flexibility, a type of plasticity that potentially could be influenced by adult neurogenesis. In this view, striatal adult neurogenesis may have evolved to provide specific types of neural plasticity in humans. Nevertheless, the functional significance of adult striatal neurogenesis remains to be established (Ernst and Frisén, 2015).

1.4 Significance of adult neurogenesis in neurodegenerative diseases

Important roles for adult neurogenesis in brain functions are started to be revealed. It has been recently demonstrated that old neurons are replaced by new neurons in the olfactory bulb, whereas neurogenesis contributes to the increase in neuronal number in the dentate gyrus in adult rats (Imayoshi *et al*., 2008). Furthermore, it has been shown that newly formed neurons are incorporated into the functional networks of both the olfactory bulb and the dentate gyrus (DG). Moreover, it has been suggested that adult neurogenesis is involved in spatial memory formation (Zhao *et al*., 2008; Vukovic *et al*., 2011).

The existence of neurogenesis in adult brain raises the possibility that the brain possesses an intrinsic regenerative potential to repair itself. Actually, many experimental studies

have highlighted that NSCs reveal the capacity to respond actively to specific pathological conditions, migrate to areas of injury and secrete neuroprotective molecules, in addition to their potential of generating a variety of new functional cells types. Indeed, adult neurogenesis increases after several acute pathologic stimuli, such as ischemia, hypoxia, seizures and stroke (Ziemka-Nalecz and Zalewska, 2012; Sawada and Sawamoto, 2012). Similarly, adult neurogenesis results altered in neurodegenerative conditions. Neurodegenerative diseases are diseases of the central nervous system characterized by a chronic and selective cell death process of neurons. These diseases, such as Alzheimer's disease, Parkinson's disease and Huntington's disease, are all characterized by a progressive and irreversible neuronal deterioration that affects selected and distinct neuronal populations, in each of these disease, leading to progressive cognitive impairment, dementia, motor disturbances and behavioral and psychological disorders that are characteristic for each of them, due to the involvement of distinct neuronal populations and circuits. The exact etiology underlying the onset of the pathology in these different neurodegenerative diseases has not been fully defined, however both genetic and environmental factors appear to play a key role. For instance, Parkinson's disease (PD) is a longstanding progressive neurodegenerative disorder characterized by the loss of dopaminergic neuron in substantia nigra (SN), in which the neuropathological characteristics are Lewy bodies and Lewy neuritis, containing the fibrillar and misfolded protein α-synuclein protein (Goedert, 2001). Huntington’s disease (HD) is a detrimental autosomal dominant neurodegenerative disorder caused and characterized by cytosine-adenine-guanine (CAG) repeated expansion within the huntingtin protein-encoding gene. HD results from the loss of GABA medium spiny projection neurons in the caudate nucleus, in addition to deterioration of specific populations of striatal interneurons. The clinical symptoms of this disease include cognitive decline, psychiatric syndromes and progressive involuntary choreatic movements (Li and Li, 2004; Walker, 2007).

Studies on adult neurogenesis performed in different animal models for neurodegenerative diseases have shown diverse and

variable results. For instance, Zhao and colleagues noted, in adult male C57 Bl/6 mice, that neurons in the dopaminergic projection, that are lost in PD, can be regenerated from stem cells (Zhao *et al*., 2003). Another study showed that there is a population of dividing neural progenitor cells (NPCs) in the young adult female Fisher 344 rats SN that can generate mature glial cells (Lie *et al*., 2002). Differently, *in vivo* BrdU labeling experiments failed to give evidence of dopaminergic neurogenesis in adult SN, since the production of new dopaminergic neurons in the SN in C57BL/6 mouse and Sprague-Dawley rat models of PD was not observed (Fielingsdorf *et al*., 2004). In this view, the impaired neurogenesis reported in both animal models of PD and PD patients may be explained as a consequence of dopaminergic denervation. In fact, dopamine plays a regulatory role in SVZ and DG neurogenesis in the adult intact brain (Hoglinger *et al*., 2004).

Regarding Huntington's disease, several studies have reported decreased proliferation in the DG of the rat model for HD. Lazic and colleagues found that there is no significant difference in hippocampal cell proliferation between R6/1 transgenic mouse model for HD and wild type controls at young age, but that this difference becomes important in older (20 weeks) animals. In contrast to the reduced proliferation in DG, proliferation in the SVZ is unchanged in mouse models of HD respect their wild type controls (Lazic *et al*., 2004; Ruan *et al*., 2014). It has been also reported that wild type huntingtin protein stimulates the transcription of BDNF, an important neurotrophic factor involved in brain development and neurogenesis, that is found down-regulated both in R6/2 transgenic mouse and rat models of HD and in HD patients (Ciammola *et al*., 2007; Conforti *et al*., 2008). In HD, the mutant huntingtin protein failed its task, causing suppressed transcription of BDNF gene. This could explain the reduced hippocampal cell proliferation in mouse models of HD (Ruan *et al*., 2014).

Finally, the different alteration of adult neurogenesis in Alzheimer's disease is discussed in the following paragraphs.

1.5 Alzheimer's disease (AD)

The Alzheimer's disease (AD) today affects about 5% of people over 60 years of age and about 40% between 85-90 years old. In 2013, there were an estimated 44.4 million people with dementia worldwide. In Europe there are about 6.4 millions of AD-affected people, and the number of AD patients in Italy is estimated around 900 thousand. This number is expected, in the absence of treatments really effective, to boost dramatically as a result of increasing in the average share of population at risk.

The Alzheimer's disease is named after Alois Alzheimer, German neurologist, who described for the first time in 1907 the symptoms and neuropathological aspects of this disease. AD is an age-related neurodegenerative disease characterized by progressive loss of memory and deterioration of cognitive functions. AD has, in general, a sneaky start: people begin to forget somethings, to get to the point which can no longer even recognize family members and need help for everyday tasks. In the early stages of AD, the hippocampus is the first area to be affected and, as a consequence, numerous patients with AD exhibit symptoms affecting learning and memory in addition to spatial and temporal orientation. The clinical manifestation of AD is seen in the domains of memory and spatial navigation in the early phases of the disease, with affection of almost all cognitive domains including executive function failure, emotional instability, psychosis and both retrograde and anterograde amnesia as the disease progresses (Amlien and Fjell, 2014; Ruan *et al*., 2014). A key feature of middle-aged and old-aged patients with AD is the progressive slow loss of axonal and dendritic arborization and finally loss of many neurons, resulting in the shrinkage of the brain. The neuronal loss is mostly marked in the hippocampus.

In Alzheimer's disease, there are two primary histopathological features evident upon post-mortem examination of brain tissue: amyloid plaques and neurofibrillary tangles. The plaques consist of insoluble extracellular deposits of amyloid-β (Aβ) peptide, while neurofibrillary tangles (NFTs) consist of aggregates of hyperphosphorilated Tau, a microtubule-binding protein. Of note, the number of neurofibrillary tangles, but not Aβ plaques, has been found to correlate with dementia.

Tau binds natively unfolded microtubules and functions in regulating their stability and axonal development and transport. As result of alternative splicing, there are several Tau isoforms, which are different for the number of microtubule-binding repeats in C-terminal region. The predominant isoforms in neurons are three (3R) and four (4R) repeat-containing Tau, that are included in the neurofibrillary tangles of AD. In patients with AD the deregulation of Tau phosphorylation and its subsequent aggregation into NFTs impairs neuronal functioning and ultimately leads to cell death (Ballard *et al*., 2011; Iqbal *et al*., 2014; Puzzo *et al*., 2014; Ruan *et al*., 2014). Molecular genetic studies have proved the central role of Aβ in the pathogenesis of AD. The Aβ peptide is liberate from a large integral membrane protein, amyloid precursor protein (APP), by sequential β- and γ-secretase cleavage. In the non-amyloidogenic pathway, α-secretase cleaves APP within Aβ domain, resulting in generation of a soluble fragment of APP (sAPPα) and a membrane-bound carboxyl-terminal fragment, thereby preventing the formation of Aβ. In the amyloidogenic pathway, the APP is cleaved at the N-terminus by β-secretase, generating a secreted ectodomain sAPPβ and a membrane-bound fragment. Cleavage of the latter product by the γ-secretase complex generates APP intracellular domain (AICD) and Aβ peptide (Fig. 6).

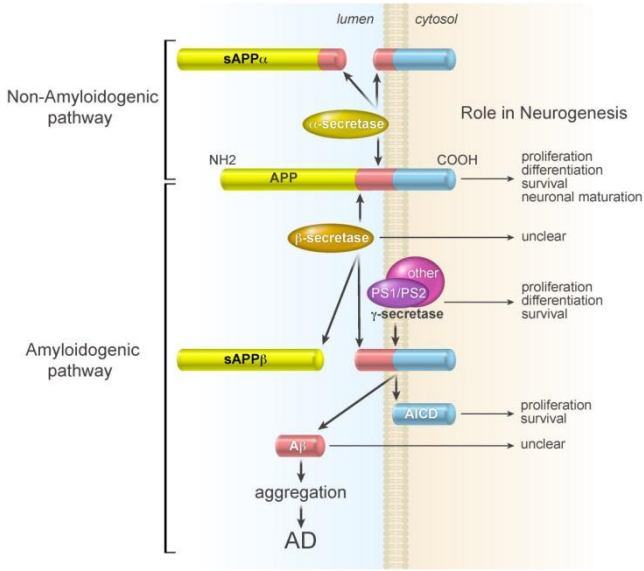

Figure 6. Molecular basis of APP processing.
In the non-amyloidogenic pathway APP is processed by α-secretase. In the amyloidogenic pathway APP is sequentially cleaved by β- and γ-secretases. (Mu and Gage, 2011)

Two main forms of Aβ are involved in AD: Aβ1-40, the 40-amino acid peptide, which is the predominant form produced by APP's metabolism, and Aβ1-42, the longer peptide, produced in least amount, but more cytotoxic and prone to aggregation than the first (Li *et al*., 1999; Ziabreva *et al*., 2006; Mu and Gage, 2011).

Aβ and Tau oligomers, as well as amyloid plaques and NFTs, share many structural and biophysical properties, such as a high β-sheet content, resistance to proteolytic degradation and neuronal toxicity (Wisniewski and Goñi, 2014). Furthermore, Aβ oligomers cause changes in spine morphology and decreases in spine density, which is relevant for underlying the cognitive impairments of AD (Selkoe, 2008).

There are two forms of Alzheimer's disease: the sporadic form, in which the presence of the ε4 allele in apolipoprotein E

(apoE4) represents the most important genetic risk factor; and the familial form (1%), characterized by mutation in the genes encoding for APP and presenilins (PS1 and PS2), which form the catalytic core of the γ-secretase complex.

The dominant theory for the causation of AD has been the amyloid cascade hypothesis. This updated theory suggests that accumulation of Aβ peptides, particularly in a highly toxic oligomeric form, is the primary pathogenic driver, that downstream leads to Tau hyperphosphorylation, NFTs formation and ultimately to synaptic and neuronal loss. The principal argument against this theory derives from many studies reporting little or no correlation between the number or size of amyloid plaques and dementia.

Extensive evidence supports the amyloid cascade hypothesis in the familial form (FAD) of AD patients and in the corresponding animal models: (*i*) inherited forms of AD linked with mutations in the APP gene or in the PRES1 or PRES2 genes are associated with changes in APP processing that facilitate over production of sAβ or production of more aggregation prone forms of sAβ such as Aβ1-42; (*ii*) Down's syndrome, where there is an extra copy of the APP gene due to trisomy 21, is associated with AD related pathology at a very early age; (*iii*) in transgenic and other models of co-expressed Aβ and Tau proteins, Aβ oligomers formation precedes and accentuates Tau related pathology, consistent with the hypothesis that NFTs formation is downstream from Aβ aggregation; (*iiii*) in transgenic mouse models of mutant APP over-expression therapeutic prevention and/or removal of Aβ is associated with cognitive benefits in experimental mice (Tanzi *et al*., 2005; Hardy *et al*., 2002; Holtzman *et al*., 2012; Lemere, 2013; Mobley *et al*., 2014).

1.6. Adult neurogenesis and AD

Since the latter stages of AD are characterized by a massive loss of neurons, possible role of adult neurogenesis in the pathogenesis of AD has been investigated. Indeed, the complete understanding of the role of neurogenesis in the pathology

would exploit this physiological process as a possible therapy for Alzheimer's disease.

Actually, studies performed in the different transgenic animal models of AD show a compromised neurogenesis in both SVZ and DG neurogenic niches, even though there are conflicting results regarding the level of neurogenesis, with a majority of studies reporting reduced neurogenesis and some others observing increased new neurons generation. For instance, increased neurogenesis has been observed in the neurogenic niches of transgenic mice for a mutant form of APP (Haughey *et al*. 2002), as well as in post-mortem brains of AD patients (Jin *et al*., 2004; Ziabreva *et al*., 2006; Hollands *et al*., 2016). On the other hand, transgenic mice with different presenilin mutations showed either increased or decreased neurogenesis (Wang *et al*., 2004; Wen *et al*., 2004; Bonds *et al*., 2015). Based on these results, different hypotheses have been formulated about the role of neurogenesis in AD. Some authors suggest that enhanced neurogenesis occurs in diseased brain as a self-repair mechanism in response to neuronal loss. In contrast with this interpretation, it has been proposed that decreased neurogenesis might contribute to the onset of neurodegeneration. In this view, the expression of AD-causing molecules would affect and deregulate adult neurogenesis, facilitating disease progression. Most of these studies analyzed adult neurogenesis in the hippocampus, the brain region controlling learn and memory, which are the main cognitive functions to be compromised in AD. It has been shown that the affected brain responds to the neuronal loss in the hippocampus by activating the dentate gyrus neurogenesis. However, due to the lack of the proper neurotrophic microenvironment in the AD hippocampus, the newborn cells are unable to differentiate into mature functional neurons. Thus, the process of the loss of neuronal/synaptic plasticity continues unstopped and is clinically expressed as progressive dementia in AD patients (Winner *et al*., 2011; Mu and Gage, 2011; Iqbal *et al*., 2014).

Regarding the SVZ, divergent results have been obtained in this neurogenic niche, where neurogenesis has been found to be either increased or decreased. For instance, Ziabreva and colleagues have shown an increase in progenitor activity in the

SVZ of AD's patients (Ziabreva *et al*., 2006). In according with this result, Sotthibundhu and his group have demonstrated that both exogenous and endogenous stimulation of SVZ precursor cell by Aβ1-42 promote neurogenesis in younger animals. Nevertheless, this effect is blocked with age, suggesting that SVZ neurogenesis could be differentially regulated during the AD progression (Sotthibundhu *et al*., 2008). In contrast, SVZ neurogenesis of adult APP-mutant mice (eleven to twelve-month-old mice) results impaired by Aβ-peptide. In fact, Haughey and colleagues demonstrated that human mutated APP mutation reduced proliferation of neural progenitor cells (NPCs) in transgenic mice, and that intraventricular administration of Aβ inhibits the proliferation of SVZ NPCs and also decreases the migration of newly produced cells into the cerebral cortex (Haughey *et al*., 2002b). Thus, despite these extensive studies, the role of adult neurogenesis in AD remains to be fully understood.

Indeed, there are increasing evidences that adult neurogenesis is under the influence of key molecules underlying Alzheimer's disease, such as the β-amyloid (Aβ) peptide. The accumulation of Aβ plaques is a key feature in the brains of AD patients and implicated in the disruption of normal cellular processes leading to neurodegeneration (Hardy and Selkoe, 2002). During disease progression, Aβ peptides assemble into various aggregation forms, ranging from dimers and oligomers to fibrils in amyloid plaques. However, the magnitude of amyloid plaque deposition in the brain correlates poorly with cognitive decline, and emerging evidence suggests that Aβ oligomers may be the major causes in this regard. However, it is still not clear how the pathophysiological environment in the AD brain, and in particular the different Aβ species, affect neural stem cell (NSC) biology and thus adult neurogenesis. A number of previous studies have tried to answer this important question by studying how diverse Ab conformers modulate NSC proliferation and differentiation (Lopez-Toledano and Shelanski, 2004; Calafiore *et al*., 2006; Heo *et al*., 2007). The results obtained are controversial, reporting that extracellular Aβ either decreases or increases proliferation, prevents or

induces neurogenesis of NSCs. These discrepancies are likely due to the different animal and cellular models used and, more important, the different Aβ species examined. For instance, a clear discrimination among the different conformers (i.e. monomers versus oligomers) was not always provided, leading to a misinterpretation of the phenomenon (Diaz-Moreno *et al*., 2013; Lee *et al*., 2013). Moreover, none of these studies explored the role of intracellular Aβ generation and oligomerization, which is one of the earliest event in AD pathogenesis.

1.7The experimental model: Tg2576 transgenic mice.

The Tg2576 mouse model was developed through transgenic insertion of hAPP695 construct carrying the "Swedish" double mutation (Lys670 →Asn and Met671 →Leu) and hamster prion protein cosmid vector into a C57B6/J x SJL mouse strain (Hsiao *et al*., 1996). This mutation is located by the β-secretase site and leads APP processing toward the amyloidogenic pathway, guiding to higher overall levels of Aβ. Consequently, the transgenic mice develop elevated brain levels of soluble Aβ1-40 and Aβ1-42 by 6-8 months of age and Aβ-containing neuritic plaques in the neocortex and hippocampus by 10-16 months. Histological analyses of the brain of aged Tg2576 mice reveal a large number of amyloid plaques associated with apoptosis, dystrophic neurons and ubiquitin.

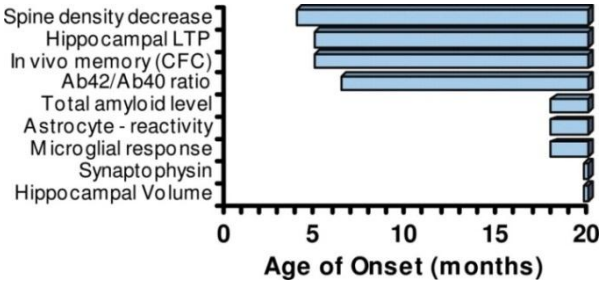

Figure 7. Temporal progression of morphological and functional deficits in Tg2576 mouse.

The earliest onset of deficits in these mice includes a decrease in hippocampal spine density and *in vivo* memory. Slower onset deficits

include an increase an amyloid load and reactive astrocytes (Jacobsen *et al*., 2006).

Similar to AD patients, Tg2576 mice do exhibit focal neuroinflammation (elevation of pro-inflammatory cytokines and microglia activation) and have an abnormal diurnal cycle with sleep abnormalities. Jacobsen and colleagues reported that neuronal deficits in Tg2576 mice are established in a time-dependent manner and can be temporally clustered into early deficits observed in 4- or 5-month-old animals. The earliest observed changes include a decrease in spine density, deficits in hippocampal neurotransmission and long-term potentiation (LTP), together with a rise in the fraction of Aβ42 in the brain (Fig. 7). The decrease in spine density is an early reflection of AD and a neuroanatomical effect of APP overexpression. Brain levels of Aβ peptide in the Tg mice increase, respect wild type controls, between 6 and 7 months, because the fraction of Aβ42 increases importantly to comprise more of 23% of the total Aβ levels. By 11-13 months of age, hemizygous mice develop numerous parenchymal Aβ plaques along with some vascular amyloid. They also show oxidative lipid damage but no evidence of neurofibrillary tangles or neuronal loss (Irizarry *et al*., 1997, Fig.8).

Figure 8. Scheme of phenotype characterization of Tg2576 mouse model (alzforum.org).

Furthermore, an increase in total amyloid load and in the number of GFAP+ astrocytes and microglia are reported in this transgenic mouse model. A recent study suggests that the intraneuronal accumulation of Aβ in distant process leads to generation of free radicals, capable to activate the mitochondrial pathway of apoptosis. Thus, Aβ causes dendritic spine loss and neuronal damage in the early stages of Alzheimer's neurodegeneration (Fig.9).

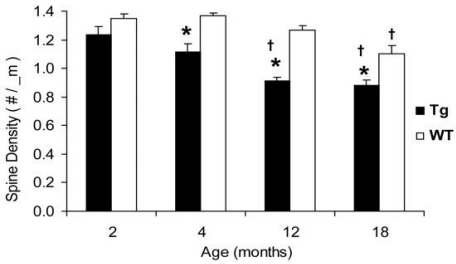

Figure 9. **Decrease in spine density in Tg mice respect to wild type controls**. It can be seen a reduced spine density detected over time in both Tg and wild type mice (Jacobsen *et al*., 2006).

From a behavioral point of view, Tg mice exhibited impairment in Y-maze alternation and several sensorimotor task compared to controls overall and particularly in an age range between 14 and 19 months (Fig.10).

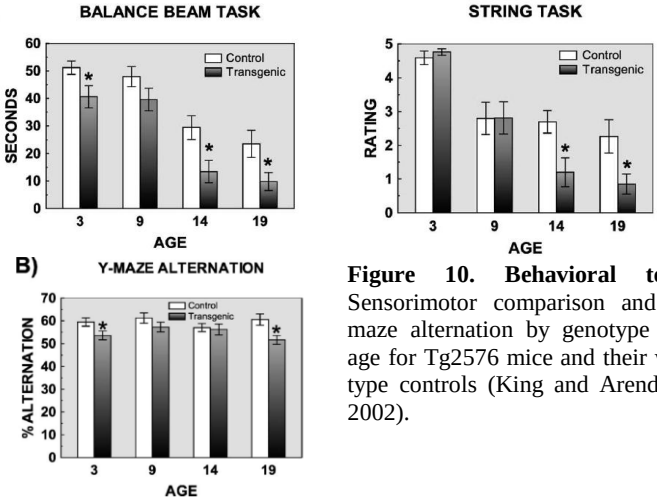

Figure 10. Behavioral tests. Sensorimotor comparison and Y-maze alternation by genotype and age for Tg2576 mice and their wild type controls (King and Arendash, 2002).

Of note, there are significant differences between the symptoms in AD and the phenotype of this model: the cognitive deficit is never so debilitating as in human patients. In these mice there is a minimal or no neuronal loss within hippocampus and cortex, and the neuron remain free of neurofibrillary tangles. Thus, this transgenic line is considered a model to study the early phase of Alzheimer's disease (Hsiao *et al*., 1996; King and Arendash, 2002; Jacobsen *et al*., 2006; D'Amelio *et al*., 2011; Bilkei-Gorzo, 2014).

One of the most commonly used technique to analyze the stem cell capacity of isolated brain cells is the neurosphere assay. *In vitro* culture of neurospheres allows for the propagation of a heterogeneous population of NSCs and their progenitors at various stages throughout development. Since its original discovery approximately 20 years ago, the assay has undergone a number of advancements. Typically, cells exhibiting stem-

like characteristics will proliferate and form clonal spheres when cultured under serum-free conditions, while those incapable of self-renewal die off following multiple passage. The addition of strong mitogens such as epidermal growth factor (EGF) and fibroblast growth factor 2 (FGF-2) allows the propagation of endogenous proliferative cells (the putative NSCs). Only 10-15% of the total cells in neurospheres are true stem cells that, after mechanical dissociation and replating, can generate secondary neurospheres (Vescovi *et al*., 2002; Gritti *et al*., 1999). Under stable culture conditions, NSCs can be long-term passaged, maintaining stable proliferation and multipotency over time (Fig.11).

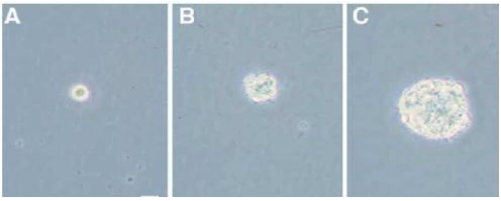

Figure 11. Neurosphere formation.
A single precursor cell (A) gives rise to one neurosphere (B) that increases in size over time (C), (Gritti *et al*., 2002).

Indeed, dissociated NSCs plated on a cell adhesion substrate, such as matrigel, and in the absence of mitogens, can differentiate spontaneously into neurons, astrocytes and oligodendrocytes (Fig.12).

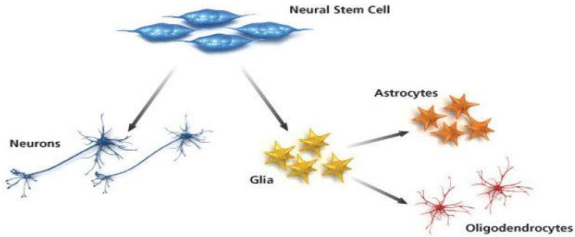

Figure 12. Multipotency of NSCs.
NSCs derived from the adult brain can be considered tripotent as they can differentiate into neurons, neurons, astrocytes and oligodendrocytes (www.sigmaaldrich.com).

1.7.1 The ScFvA13 nanobody: conformational-selective interference of AβOs

One important task of this work is to selectively target the Abeta oligomers (AβOs), that are presently considered the most neurotoxic Ab species in the AD pathogenesis. In our group it was previously developed, a recombinant single-chain antibody fragment, namely the ScFvA13 nanobody, that has been generated by a direct intracellular selection of functional intrabodies in yeast cells against the *in vivo* misfolded antigen Aβ13 (Meli *et al*., 2009). The ScFvA13 intrabody intercepts AβOs in a conformational and selective manner and, like a chaperone-protein, unfolds them in the non-toxic monomeric form (Fig. 13). A variant of this intrabody, the ScFvA13KDEL, expresses a KDEL sequence that allows its cellular localization at the endoplasmatic reticulum (ER), that is considered the putative site of Ab oligomerization and thus AβOs formation. Meli and colleagues demonstrated that ScFvA13KDEL intrabody selectively intercepts critical AβO conformers and interferes with their 'toxic' assembly occurring in the ER, without altering the complex processes of maturation and processing of APP (Meli *et al*., 2014). In this work I took advantage of scFvA13 both as an intrabody and as an nanobody, in order to operate a selective interference of both intracellular and extracellular AβOs.

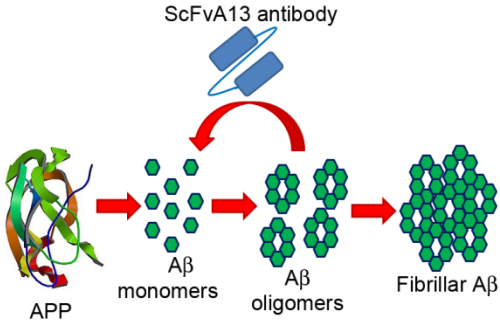

Figure 13. Scheme of APP amyloidogenic pathway and the A(beta)Os interference triggered by ScFvA13 nanobody.

In the first case, I expressed the ER-retained version of the A13 intrabody in the aNSCs, by subcloning it into a lentiviral vector (see Material and Methods for details). In the second case I administered ScFvA13 nanobody to the cell culture ad different concentration, as described in the Results section.

2.Aim of the thesis

Conflicting observations have been reported regarding the level of neurogenesis in animal models of Alzheimer's disease, as reported before. Therefore, the contribution of neurogenesis to the pathology of AD needs further clarification.

The aim of this thesis is to define how neurogenesis is regulated in Alzheimer's disease and if alterations in adult neurogenesis represent an early event in AD pathogenesis. To better address this aim I analyzed the proliferative and differentiative features of resident and SVZ- and DG-HP-derived adult neural stem cells (aNSCs) in Tg2576 transgenic mice, a well-characterized animal model of AD and Aβ accumulation. These mice offer the opportunity to analyze the early stages of the AD pathology and thus to correlate possible alterations of adult neurogenesis to the onset of the disease. Moreover, since in these mice there is an overproduction of Aβ oligomers (AβOs) in the nervous system, I investigated if naturally occurring Aβ oligomers (AβOs), which represent the most neurotoxic species in AD, modulate NSCs biology, in view of possible cross-interaction between impaired neurogenesis and the amyloidogenic processing pathway. SVZ- and DG-derived aNSCs have been analyzed *in vitro* for their proliferation and differentiation potential in relationship with the biochemical profile of the different Aβ species. I took advantage of a recombinant nanobody probe selectively binding AβOs in a conformational-and sequence-specific manner (Meli *et al*., 2009), that when expressed as an intrabody retained in the endoplasmic reticulum specifically intercepts endogenous biologically-active AβOs conformers and lead to their functional silencing (Meli *et al.*, 2014). Moreover, in order to analyze also the role of extracellular AβOs accumulation, that leads to a Aβ plaques formation at the last stage of AD, Tg2576 aNSCs have been treated with the recombinant nanobody. In this way, I could explore the causal role of AβOs in modulating NSC biology and adult neurogenesis prior to the onset of overt neurodegeneration. The ultimate goal of this research is to gain new insights into the molecular mechanisms that control adult neurogenesis in AD neurodegeneration and to develop new strategies to restore normal neurogenesis specifically in those brain regions where it

is impaired. This information will be of great benefit for the identification of competent human stem cells with similar potential and, thus, for the development of cell-replacement strategies for the cure of Alzheimer's disease and, on the other hand, for the identification of new clinical early marker of AD diagnosis.

3. Results

3.1 Olfactory bulbs neurogenesis is impaired in pre-symptomatic Tg2576 mice

Tg2576 mouse model is a slow progressive mouse model developing amyloid-beta (Aβ) plaques and deficits in learning and memory at 9–13 months of age (Hsiao *et al*., 1996; Kim *et al*., 2012). To identify alterations of adult neurogenesis at a very early prodromal stage of AD pathology, I first measured the proliferative rate of SVZ neural stem cells (NSCs) in 1.5-2 months old animal by *in vivo* BrdU labeling. Anti-BrdU staining, performed on brain sections encompassing the entire SVZ, revealed less BrdU positive cells in Tg2576 SVZ, compared to control mice (Fig. 14A, upper panels, quantified in Fig 14B; number of positive cells/mm^2 SVZ: Tg2576 271±4; WT 389±2, p>0,05), indicating a reduced proliferation of resident Tg2576 SVZ progenitors. Consistent with this data, olfactory bulb neurogenesis was also affected (Fig. 14D), with a significant decrease of newborn neurons, as quantified in Fig 14E (n° of NeuN+/BrdU+ cells/mm^2 OB: Tg2576 24.28±7.57; WT 38.56±12.27¸ p>0.001). In particular, I found less Calretinin positive interneurons in Tg2576 olfactory bulbs (n° of Calretinin+/BrdU+ cells/mm^2 OB: Tg2576 1.3±0.15; WT 3.3±0.19; p>0.05, Fig. 14E), while no significant difference in Calbindin positive neurons was found between the two genotypes (Fig.15). I also analyzed the expression of progenitors and neuroblasts markers, such as Sox2, GFAP and Doublecortin (Dcx). Immunofluorescence in Fig. 14A shows that in Tg2576 SVZ there is a significant reduction in the number of Sox2 and GFAP positive cells, while Dcx+ neuroblasts are more represented, compared to wild-type (WT), as quantified in Fig. 14C. The neurogenic defects of OB interneurons in Tg2576 could thus reflect impairment both in progenitor proliferation and in the neuronal maturation of SVZ neuroblasts. To test these hypotheses, I analyzed *in vitro* the biology of Tg2576 NSCs, as described below.

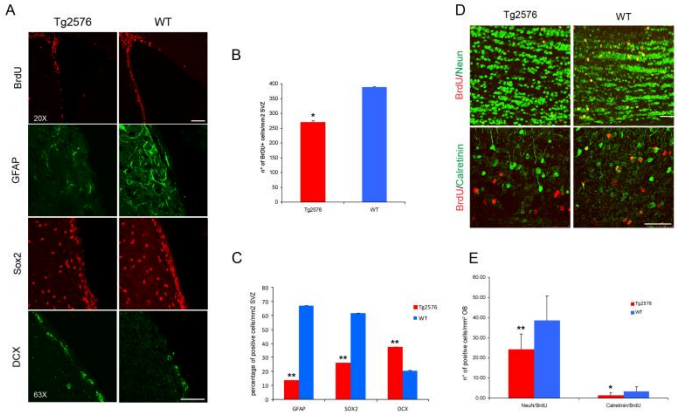

Figure 14. *In vivo* SVZ and OB neurogenesis is affected in Tg2576 mice.

A) Immunofluorescence staining for BrdU, progenitors and neuroblasts markers in adult SVZ of Tg2576 and WT mice. Immunostaining for incorporated BrdU in progenitor cells shows reduced proliferation in Tg2576 SVZ niche (red signal in top panels), while there is a significant reduction of NSCs compartment ($GFAP^+$ and $Sox2^+$cells) and an increase in Dcx^+ neuroblasts. Scale bar 100µm, 20X magnification (for BrdU) and 50µm, 40X magnification, zoom 1.9 (for SVZ markers). B-C) Quantification of BrdU (B) or Sox2, GFAP and Dcx positive cells (C) in Tg2576 (red) and control (blue) SVZ. D) Immunostaining for BrdU and NeuN (red and green respectively, top panels, 63X magnification) and BrdU and Calretinin (red and green respectively, bottom panels, 40X magnification) shows a significant reduction of newborn $CalR^+$ interneurons in Tg2576 olfactory bulbs compared to WT. Scale bar 50µm. E) Quantification of double positive cells in Tg2576 (red) and WT (blue). Data are means ± SEM of five individual animals (n=5) for each experimental group. * $p<0.05$, ** $p < 0.01$, significantly different from WT, Student's t-test.

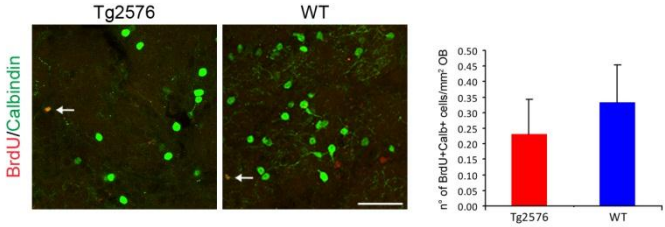

Figure 15. Deficit in olfactory bulbs neurogenesis in Tg2576 mice. Immunostaining for BrdU and Calbindin (red and green, respectively) shows nonsignificant difference in the number of newborn CalB+ interneurons (indicates by white arrows) in Tg2576 olfactory bulbs compared to WT, as quantified in the histogram on the right. Scale bar 50μm, 40X magnification. Data are means + SEM of five individual animals (n=5) for each experimental group.

3.2 Tg2576 neural stem cells proliferation and differentiation defects correlate with Aβ/ AβOs levels

To evaluate the proliferative and differentiative properties of Tg2576 neural progenitors I derived aNSCs from the adult SVZ region of 1.5 months old Tg2576 and WT mice and grew them as neurospheres cultures. Two pools of 5 SVZ dissections for each genotype gave rise to two Tg2576 and two WT neurospheres cultures (namely Tg1, Tg2 and WT1, WT2).

The overall number of primary neurospheres obtained from Tg2576 mice was significantly lower than that from WT animals (Fig. 16A-B). Moreover, the majority of Tg2576 neurospheres had a smaller size, compared to their control counterpart (average diameter of neurospheres: Tg2576 6±1.73 μm; WT 13±3.49 μm, Fig. 16B). This could reflect either a proliferative impairment of the SVZ progenitors and/or a reduction in the number of NSC resident in the SVZ, as observed *in vivo*. Indeed, Tg2576 neurospheres contained more Dcx+ neuroblasts and less Sox2 progenitors (Fig. 17A), in agreement with the *in vivo* data. Moreover, growth curves performed on Tg2576 and WT NSC at early passages (see Materials and Methods for details) showed that Tg2576 NSCs proliferated significantly much less than WT progenitors, with an average 8-fold difference (Fig. 16C).

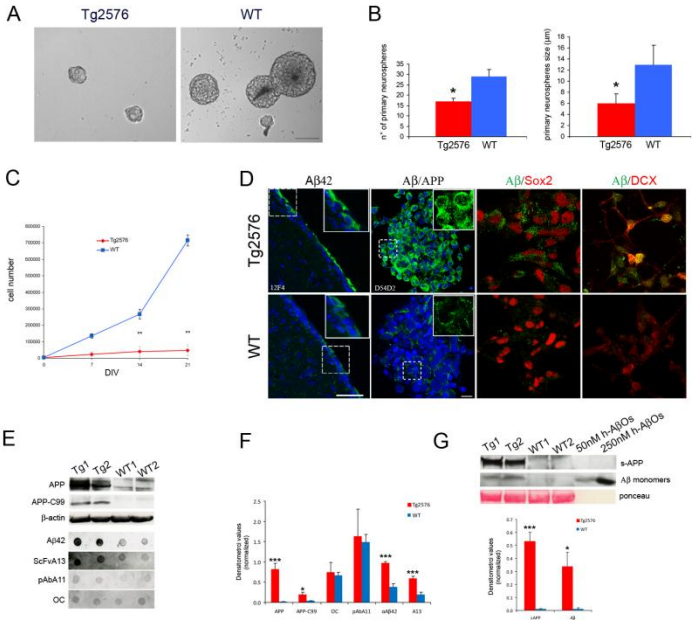

Figure 16. Reduced proliferation of Tg2576 adult neural stem cells correlates with high levels of APP and AβOs expression.

A) Phase-contrast micrograph of NSCs culture showing less primary neurospheres in Tg2576, that are also smaller in size, compared to WT. Scale bar 25µm, 10X magnification. B) Quantification of the number of primary neurospheres and of their size are expressed as mean ± SEM of five individual animals (n=5) for each experimental group. * $p<0.05$, significantly different from WT, Student's t-test. C) Cell proliferation is reduced in Tg2576 progenitors. Growth curves at early passages shows a significant decrease in proliferation of Tg2576 progenitors (red line) compared to WT sample (blue line). D) Immunofluorescence staining for Aβ42 in resident and SVZ-derived progenitors and neuroblasts markers in adult SVZ of Tg2576 and WT mice. In Tg2576 SVZ Aβ42 is highly expressed, compared to controls (green signal). Double immunostaining for APP/Aβ (green signal) and progenitors or neuroblasts/neuronal markers (red signal) in primary neurospheres, showing APP/Aβ expression in both $Sox2^+$ progenitors and Dcx^+ neuroblasts in Tg2576 neurospheres but not in WT samples. DAPI staining on nuclei in blue. Scale bar 50µm, 40X magnification,

zoom 1.9 (SVZ) and 10µm, 63X magnification, zoom 2.5 (neurospheres and cells). White square boxes in top panels represent 2X magnification of the corresponding dot-lines insets. E-G) Aβ and APP are highly expressed in Tg2576 neurospheres. E) Western blot (anti-Aβ WO2) and dot blot analysis of Tg2576 (n=5) and WT (n=5) lysates (left panel) demonstrate that human APP, APP C-99 and AβOs are almost exclusively detected in Tg2576 samples, as quantified in the histogram on the right (F). Comparable results are obtained by Western blot analysis of conditioned media (G), in which s-APP and Aβ monomers (4 KDa) are detectable only in Tg2576 media. The histogram below reports the quantification of s-APP and Aβ monomers. Quantifications are obtained from densitometric values of bands and normalized for β-actin (cell lysates) or for one band of Ponceau (conditioned media). Data are mean ± SEM of 3 independent experiments. * $p < 0.05$, ** $p < 0.01$, *** $p<0.001$ significantly different from WT, Student's t-test.

These results have been confirmed also by measuring the expression of the pan-proliferative marker Ki67 and BrdU incorporation after 2 hours of *in vitro* BrdU labeling. Double immunostaining for Ki67 and BrdU, 24 hours after the BrdU pulse, showed that the percentage of proliferating $Ki67^+$ $BrdU^+$ double positive cells was significantly lower in Tg2576 respect to WT (Fig. 17B-C), suggesting a slower cell cycle rate of Tg2576 cells, also because no difference was found between the two populations in terms of number of apoptotic cells, measured by activated-capsase-3 expression (Fig. 17D).Despite the absence of amyloid-plaques deposition in the brain parenchyma at this early age, I asked whether what I observed *in vitro* was due to Aβ produced in resident and SVZ-derived NSCs. Immunostaining of brain sections of 1.5-month old Tg2576 mice with 12F4 antibody (recognizing the C-terminal specific $A\beta_{42}$ neoepitope) shows that peptide $A\beta_{42}$ is highly present along the entire SVZ, already at this presymptomatic age (Fig. 16D). As well, immunostaining on primary neurospheres with D54D2 antibody (preferentially recognizing human APP (hAPP) and human Aβ (hAβ) with respect to the mouse counterpart), confirmed that Tg2576 neurospheres express the transgenic hAPP and produce hAβ also *in vitro* (Fig. 16D).

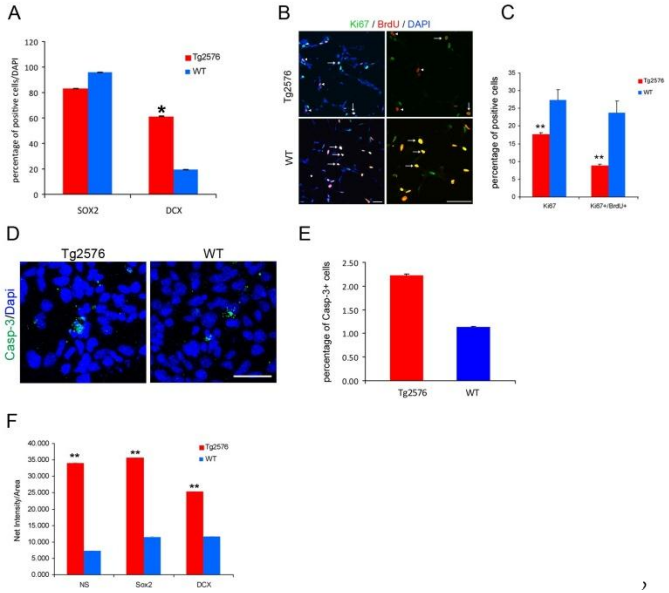

Figure 17. Cell composition of Tg2576 SVZ neurospheres.
A) Quantification of Sox2 and Dcx positive cells in Tg2576 (red) and control (blue) SVZ. *In vitro* analyses report a reduction of aNSCs compartment (Sox2+cells) and a significant increase in Dcx+ neuroblasts, confirming the *in vivo* data. Data are means + SEM of five individual animals (n=5) for each genotype. * $p<0.05$, significantly different from WT, Student's t-test. B-C) Double immunofluorescence for BrdU (red signal) and Ki67 (green) shows the lower percentage of double positive proliferating cells (yellow arrowhead) in Tg2576 neurospheres compared to WT, as quantified in C. DAPI staining on nuclei in blue, 40X magnification, zoom 1.25 right panels, scale bars 50µm and 75µm, respectively. D-E) No difference in apoptosis between the Tg2576 and WT progenitors. D) Immunostaining for cleaved caspase-3 (green signal) shows that there is not a significant difference in apoptosis between Tg2576 and WT samples, as quantified in the histogram in E. DAPI staining on nuclei in blue. Scale bar 50µm, 63X magnification. Data are means + SEM of five individual animals (n=5) for each experimental group. F) Quantification of immunofluorescence intensity of APP/Aβ-expressing cells (n=50) in neurospheres and for each type of progenitor and

neuroblasts markers, as mean ± SEM of the analysis of 3 independent experiments.

In particular, hAPP/Aβ is highly detected in both Sox2+ progenitors and Dcx+ neuroblasts (Fig 16D). Western blot analysis shows high levels of full length APP and APP-C99 terminal fragment in Tg2576 neurosphere cell extracts (Fig. 16E), and high levels of soluble-APP and Aβ monomers in Tg2576 neurosphere-derived conditioned media (Fig. 16G). This result confirms the maintenance *in vitro* of the amyloidogenic pathway in the Tg2576 neurosphere cells. To better characterize the pattern of Aβ species in native conditions, I performed Dot-blot (DB) analysis, demonstrating that Tg2576 neurospheres produce high levels of intracellular Aβ42, compared to WT cells. Notably, DB performed with conformational antibodies shows in Tg2576 samples a selective overproduction of intracellular AβOs (Fig. 16E) detected by the oligomeric-specific scFvA13 nanobody (Meli *et al*., 2014) but not of other conformers (such as generic pre-fibrillar or fibrillar oligomers, respectively recognized by A11 or OC polyclonal antibodies) (histogram in Fig. 16F). In addition to the proliferative defect of Tg2576 SVZ progenitors, an impairment of their differentiation into olfactory interneurons could also participate in generating the observed OB phenotype of Tg2576 mice. To address this point, I tested the differentiation potential of Tg2576 neural progenitors *in vitro*, by measuring the expression of the neuron-specific class III b-tubulin (TuJ1) and astrocytes marker GFAP, upon neurospheres dissociation and differentiation (see Materials and Methods section). Immunofluorescence staining for TuJ1 and GFAP (red and green signal on Fig. 18A, respectively) in Tg2576 and WT differentiated neurospheres showed that Tg2576 neurons are poorly differentiated, with very short neuritic processes (as quantified in Fig. 18C), while GFAP+ cells displayed an altered cell shape, as they lose the bushy-like morphology, typical of astrocytes, and displayed an elongated shape with few ramifications.

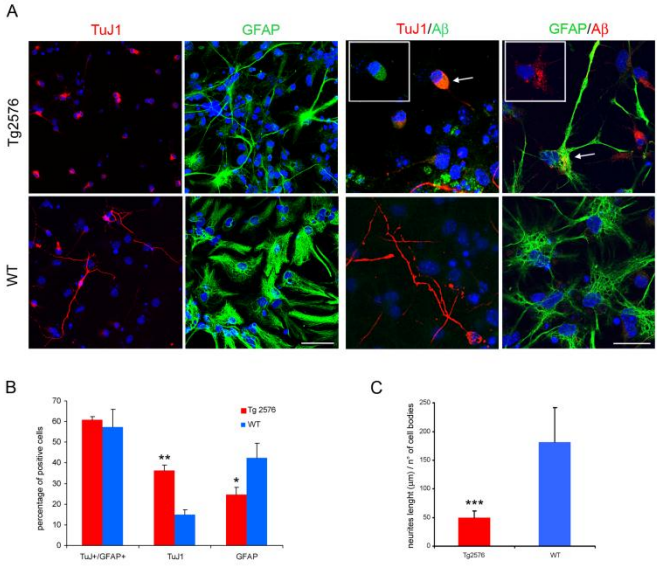

Figure 18. Differentiative impairment of Tg2576 aNSCs.
A) Immunostaining for TuJ1 (red) and GFAP (green) shows that Tg2576 neurospheres give rise to more $TuJ1^+$ neurons at the expense of $GFAP^+$ astrocytes, as quantified in B. Both Tg2576 neurons and astrocytes express higher level of Aβ than their control counterpart (green and red signal, respectively, in the white square boxes with the corresponding cell indicated by the arrows), and fail to differentiate properly, as shown by the drastic reduction of neurites and the dystrophic cell shape of astrocytes. Scale bar 50µm, 40X magnification, zoom 1.5 for the left panels and scale bar 20µm, 63X magnification, zoom 2 for the other panels. C) Quantification of length filaments per number of neuron bodies in Tg2576 (red, n=7) and control (blue, n=7) samples is expressed as mean ± SEM of 3 independent experiments. *** $p<0.001$ significantly different from WT, Student's t-test. C) Quantification of percentage of positive ($TuJ1^+$ or $GFAP^+$) cells in Tg2576 (red, n=5) and WT (blue, n=5) samples is expressed as mean ± SEM of 3 independent experiments. ** $p< 0.01$ (for $TuJ1^+$ neurons) * $p < 0.05$ (for $GFAP^+$ astrocytes), significantly different from WT, Student's t-test.

This phenotype was also detectable *in vivo* in the neurogenic niche (Fig. 19), suggesting that the glial defect observed in the differentiated neurospheres cultures is due to an intrinsic defect of the astrocytes progenitors. Moreover, the majority of the Tg2576 progenitors produced TuJ1+ cells, while WT cells gave rise mainly to GFAP+ astrocytes (Fig. 18B). The increased number of TuJ1+ cells in Tg2576 cultures well correlates with the higher number of Dcx+ neuroblasts found *in vivo*, and occurs at the expense of the glial compartment, as the number of GFAP+ cells is reduced in Tg2576, whereas the percentage of the overall differentiated cells (neurons and astrocytes) does not change between transgenic and WT animals (60,8% vs 57,5%, Fig. 18B). This data strongly suggests that both neuronal and glial defect observed in the differentiated neurospheres cultures could be due to an intrinsic defect of the SVZ progenitors, probably caused by the overproduction of Aβ. To test this hypothesis, I first analyzed the amount of Aβ in neurons and astrocytes derived from the progenitors, by performing double immunostaining for TuJ1 or GFAP and Aβ. Interestingly, both Tg2576 neurons and astrocytes showed high level of Aβ, compared to WT differentiated cells, which were not immunoreactive for the D54D2 anti-hAβ antibody (Fig. 18A). I can thus conclude that total Aβ (oligomers + monomers) accumulation in progenitors and differentiated Tg2576 cells well correlates with their severe proliferation and differentiation defects and suggests a cell-autonomous defect.

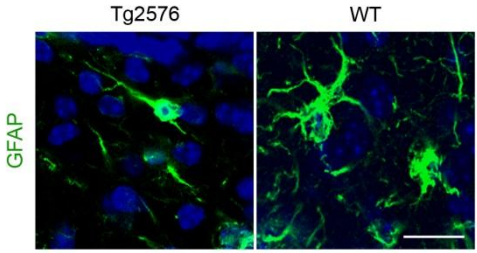

Figure 19. Altered astrocytes morphology in Tg2576 SVZ.
Immunofluorescence staining for GFAP (green) shows an evident altered elongated cell shape of Tg2576 astrocytes, respect their control

counterpart, in the SVZ *in vivo*. DAPI staining on nuclei in blue. Scale bar 10 µm, 63X magnification.

3.3 Intracellular interference with Aβ oligomers rescues proliferative and differentiative defects of Tg2576 aNSCs

I have previously demonstrated that the intracellular expression of the scFvA13 anti-AβOs in the endoplasmic reticulum (ER) allows a conformational selective and subcellular ER localized interference of AβOs pools but not of Aβ monomers nor of the APP processing or trafficking (Meli *et al.*, 2014). In particular, scFvA13-KDEL intrabody targets intracellular AβOs in the endoplasmic reticulum and interferes with the cellular pathways leading to their formation and actions. Here, in order to investigate if endogenous AβOs were responsible for the proliferative and differentiative impairment of Tg2576 progenitors in a cell-autonomous manner, I expressed in these cells the scFvA13-KDEL intrabody (Meli *et al.*, 2104). To express the scFvA13-KDEL intrabody in neurospheres, I generated the pLentiA13K_GFP lentivirus (see Materials and Methods and construct map in Fig. 20A). The expression of transduced intrabody was detected by immunofluorescence either 5 days after infection in progenitors or 12 days after infection in differentiated neurons and astrocytes (Fig. 21A). The subcellular localization of scFvA13-KDEL in the ER was confirmed by the double immunostaining for V5 and the ER marker Calnexin (red and green signal, respectively, in Fig. 21A), and its effective enrichment in the ER was further demonstrated by electron microscopy (Fig.20B) and through the immunoprecipitation analysis of microsome extracts (Fig. 20C).

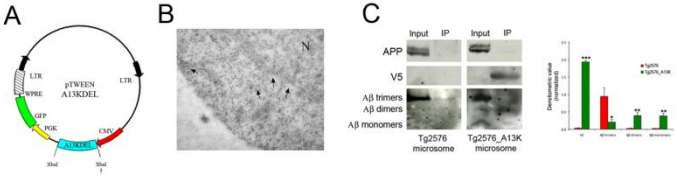

Figure 20. Impact of scFvA13-KDEL expression in Tg2576 aNSCs.

A) Plasmid map of pTWEEN A13K-DEL vector used to generate the lentiviral particles. The bicistronic plasmid, carrying the GFP sequence

under the PGK promoter, contains the scFvA13-KDEL cDNA cloned downstream the CMV promoter and upstream the PGK_GFP cassette. B) Electron microscopy confirmed that the ScFvA13_KDEL intrabody is expressed in the endoplasmic reticulum in Tg2576 infected NSCs, as indicated by the black harrows. C) Intrabody-mediated selective pull-down of AβOs: co-IP of scFvA13-KDEL intrabody with Aβ dimers, Aβ trimers but not with APP and Aβ monomer, from microsome of Tg2576_A13K cells and not from Tg2576. The co-IP was performed by using an anti-V5 coupled resin to bind the C-terminal V5 tag of the intrabody, and then blotted with mAb D54D2 and mAb WO2 to detect the different Aβ species and APP, respectively, and with anti-V5 for the intrabody detection. On the right, the histogram represents the quantification of the representative Aβ and V5 bands detected and normalized for APP.

WB analysis showed that the steady-state levels of full-length APP and of APP C-terminal fragments (CTFs) in total lysates, as well as of soluble α-APP and β-APP in the extracellular medium (Fig. 21B,C), are similar in Tg2576 and Tg2576_A13K cells. Moreover, DB analysis showed that in Tg2576 infected progenitors (Tg2576_A13K) the scFvA13-KDEL intrabody expression significantly and selectively reduced the levels of intracellular Aβ42 and scFvA13-positive AβOs (Fig.21D) and of extracellular scFvA13-positive AβOs (Fig.21E) to those measured in WT progenitors. In addition, the levels of intracellular conformers measured by the other antibodies (namely A11 and OC pAbs) remained unchanged (Fig. 21D). Of note, these results provide a further confirmation of the conformational selective interference (CSI) with AβOs, mediated by scFvA13-KDEL intrabody (Meli *et al.*, 2014) also in the Tg2576 neurosphere model.

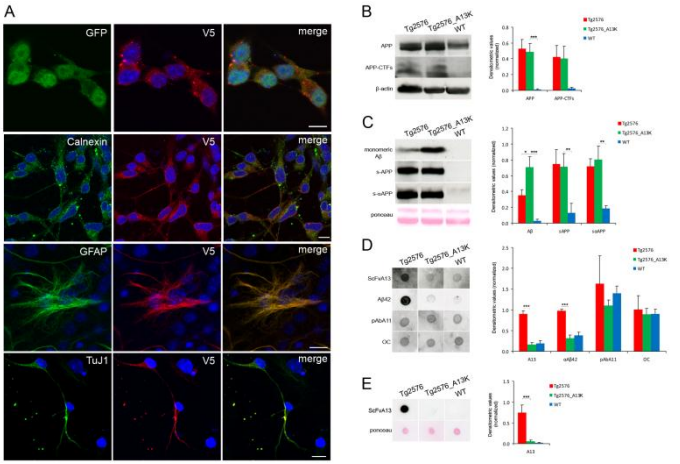

Figure 21. Impact of scFvA13-KDEL in Tg2576 aNSCs on the intra-and extracellular patterns of Aβ species.

A) Tg2576 infected GFP+ progenitors (Tg2576_A13K, green signal, left panel) stably express scFvA13-KDEL intrabody, as shown by immunofluorescence staining for its C-terminal V5 tag (red and merged signal in central and right panels, respectively). The co-localization of V5 (red) with the ER marker Calnexin (green) demonstrates the ER localization of the intrabody (merged signal in right panel). scFvA13-KDEL expression (in red, central bottom panels) is maintained upon differentiation of the progenitors into Tuj1 + neurons and GFAP+ astrocytes (green and merged signal in left and right bottom panels, respectively). Scale bar 10μm, 63X magnification, zoom factor from top to bottom panels: 2.5 (GFP/V5 staining), 2 (Calnexin/V5 staining) and 3.5 (TuJ1/V5 and GFAP/V5 staining). B-C) Western blot for full-length APP (anti-APP C-terminal) and for APP-CTFs, as well as for soluble APP (s-APP, anti-APP WO2) and soluble α-APP (sα-APP, anti-APP N-terminal 22C11) in Tg2576, WT and Tg2576_A13K lysates (B) and conditioned media (C) indicates that scFvA13 does not affect the processing of APP in the aNSCs, as quantified by the densitometric values reported in the corresponding histograms on the right. D-E) Dot Blot analysis on lysates (D) and conditioned media (E) shows that the stable expression of scFvA13-KDEL intrabody reduces the amount of AβOs to levels comparable to those measured in WT samples. Histograms on the right represent the quantification of the corresponding western and dot blots on the left,

normalized for β-actin (for lysates, B and D) or Ponceau (for conditioned media, C and E)

Strikingly, scFvA13-KDEL expression rescued both the proliferative impairment and the differentiation defects of Tg2576 progenitors (Figure 22).

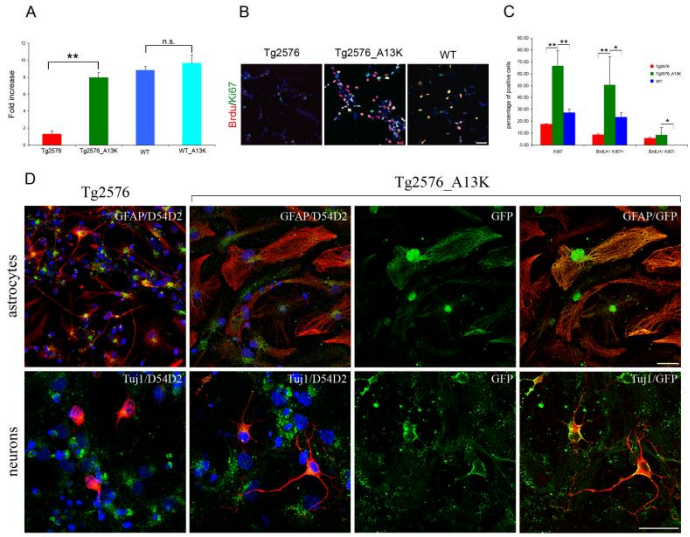

Figure 22. scFvA13-KDEL intrabody rescues the proliferative and differentiative impairment of Tg2576 aNSCs.
A) Growth curve of aNSCs (Tg2576, Tg2576_A13K, WT and WT_A13K, n=3) shows that the stable expression of scFvA13_KDEL intrabody lead to an undeniable rescue of the proliferative defect of Tg2576 progenitors, while does not influence proliferation of WT cells. Differences in proliferation rates are expressed as fold increase (FI), as mean ± SEM of 3 independent experiments. ** $p < 0.01$, significantly different from Tg2576, Student's t-test), as reported in the histogram on the right. B-C) Immunostaining for BrdU (red) and Ki67 (green) shows that in Tg2576_A13K samples there are more $BrdU^+$ and double $BrdU^+/Ki67^+$ cells, confirming the rescue of proliferation of Tg2576 aNSCs by scFvA13-KDEL. Scale bar 50µm, 63X magnification. C) Quantification of percentage of $BrdU^+$ cells, $Ki67^+$ cells and double positive ($BrdU^+/Ki67^+$) cells in Tg2576 (n=3), Tg2576_A13K (n=3) and WT (n=3) samples is expressed as mean ±

SEM of 3 independent experiments. ** $p < 0.01$ (Ki67 $BrdU^+/Ki67^{+)}$, significantly different from Tg2576, and * $p < 0.05$ ($BrdU^+/Ki67^+$ and $BrdU^-/Ki67^+$) and ** $p<0.01$ (Ki67) significantly different from WT, Student's t-test. D) Immunofluorescence staining for GFAP (red, top panels) and TuJ1 (red, bottom panels) shows that in Tg2576_A13K sample the expression of scFvA13 intrabody (GFP^+ cells) leads to a partial rescue of the dystrophic shape of astrocytes (top panels), while a more robust rescue of neurons maturation and arborization is evident. Scale bar 25µm, 63X magnification, zoom 1.3 and 2.5 (top and bottom panels, respectively).

Cell proliferation of Tg2576_A13K, as analyzed by growth curves, Ki67 expression and BrdU incorporation, was comparable to that of WT cells (Fig.22 A-C), and this effect of the intrabody did not depend on a difference in the percentage of apoptotic cells (Fig 23.) Both glial and neuronal morphology was restored to the WT phenotype, despite the persistent expression of Aβ in the culture (Fig.22 D).

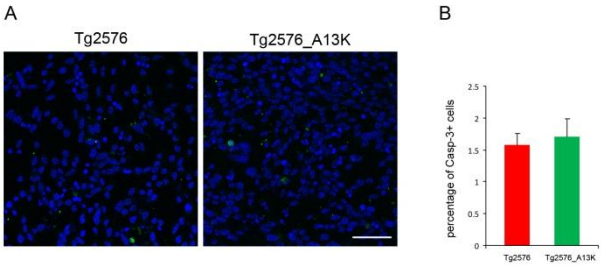

Figure 23. No difference in apoptosis between Tg2576 and Tg2576_A13K *ex vivo* progenitors.
A) Similar percentage of apoptotic cells are present in Tg2576 and Tg2576_A13K progenitor populations, as shown by the immunostaining for cleaved activated caspase-3 (green signal) and the quantification in the histogram (B). DAPI staining on nuclei in blue. Scale bar 50µm, 63X magnification. Data are means + SEM of five individual animals (n=5) for each experimental group.

The effect of scFvA13_KDEL intrabody was particularly appreciable in neuronal differentiation, since neurites length of Tg2576_A13K neurons was comparable to that of WT cells, as measured in Fig. 24.

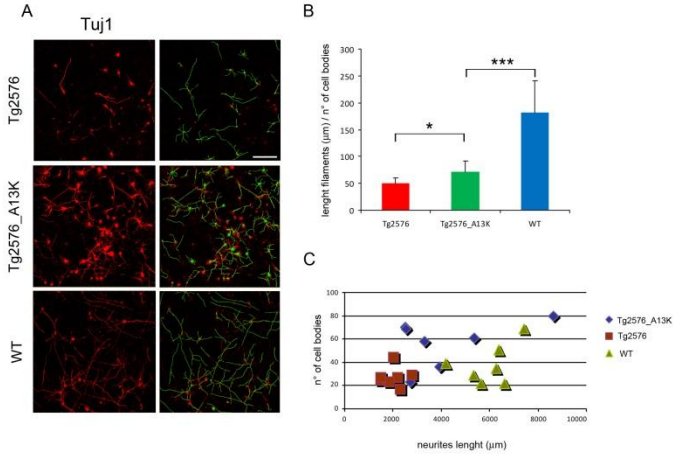

Figure 24. Rescue of neuronal differentiation of Tg2576 progenitors by scFvA13_KDEL intrabody expression.
A) Immunofluorescence staining for neurons (TuJ1, red signal) highlights scFvA13-KDEL intrabody effect on the degree of Tg2576 neuronal maturation. In fact, in Tg2576_A13K samples, neurites length is comparable to those measured in WT sample, as quantified in the histograms in B and C. Scale bar 25µm, 40X magnification, zoom 1.5. Data are means + SEM of five individual animals (n=5) for each experimental group.

3.4 Morphological differentiation defects of Tg2576 neurons are due to AβO-dependent hyperstabilization of microtubules

Neurons derived from Tg2576 neurospheres are poorly differentiated, with very short neuritic processes (Fig.18). Neuronal morphology strictly relies on the organization of the cytoskeleton and the microtubule-associated-protein(s) (MAP) tau is known to regulate the microtubule dynamics in living neurons (Conde and Caceres, 2009; Janning *et al*., 2014). I investigated the dynamic state of microtubule network in WT, Tg2576, and Tg2576_A13K neurospheres by evaluating the site-specific phosphorylation of tau, and the related acetylation and tyrosinylation of α-tubulin (Johnson and Stoothoff, 2004). WB analysis shows a dramatic downregulation in phospho-tau (AT8),

together with a reciprocal increase in non-phospho Tau-1 immunoreactivity in Tg2576 aNSCs, compared to WT control. As well, Tg2576 aNSCs display a significant up-regulation of acetyl-αtubulin (stable) with a downregulation of tyrosinylated-αtubulin (instable). The overall results are in line with a pattern of hyper-stabilized microtubules. Interestingly, scFvA13-KDEL antibody expression in Tg2576 neurospheres induces a massive increase of tau phosphorylation (AT8) coupled with a significant decrease of Tau1.

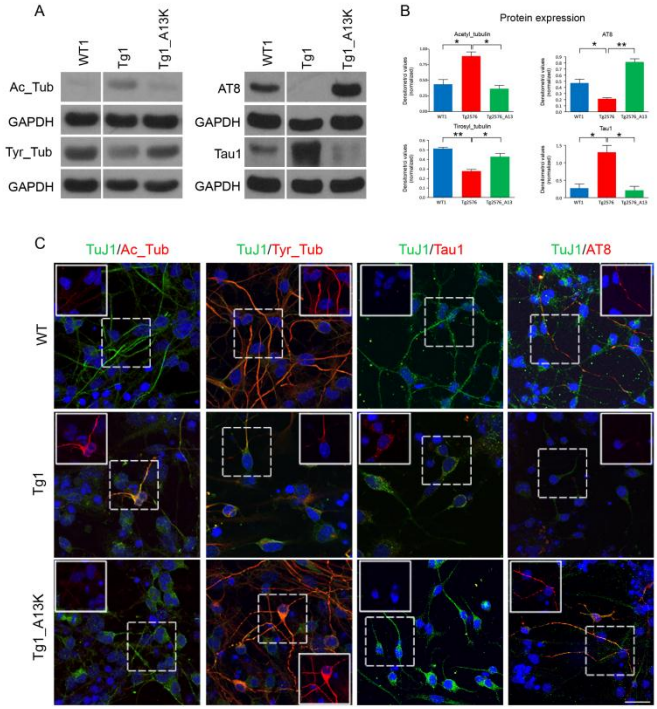

Figure 25. Rescue of cytoskeleton alteration in Tg2576_A13 aNSCs.

A) Western blot analysis of Tg2576, Tg2576_A13K and WT cell lysates with antibodies against acetyl (stable) - and tyrosinylated (instable) - αtubulin and against the Tau1/AT8 epitopes. Tg2576 aNSCs display hyper-stable microtubules, as indicated by the important up-regulation in acetyl Tub-positive microtubules (left

panel) and the dramatic downregulation in AT8 tau immunoreactivity (right panel). Interestingly, the stably expression of scFvA13 intrabody is able to significantly rescue the cytoskeleton alteration, normalizing the microtubule instability to physiological control levels. B) Densitometric quantification of the acetyl-αtubulin, tyrosinylated-αtubulin, AT8 and Tau1 intensity bands in Tg2576 (red), Tg2576_A13K (green) and WT (blue) samples—was calculated normalizing for GAPDH used as loading internal control. Data are means ± SEM of 3 independent experiments. * $p<0.05$, ** $p<0.01$, significantly different from WT, Student's t-test. C) Immunofluorescence staining for neurons (TuJ1, green signal) and the two forms of αtubulin or Tau1/AT8 epitopes (red signal) confirms the Western blot results. The higher level of acetyl-αtubulin and of phosphorylated tau in Tg2576 samples are rescued at level comparable to those measured in WT by the stable expression of anti-AβOs intrabody. DAPI staining on nuclei in blue. Scale bar 25μm, 63X magnification, zoom 1.5. White squared boxes represent only the red signal of the corresponding dot-lines insets.

Moreover, I observed a significant decrease of acetylation of tubulin mirrored by an increase of its tyrosinylation. Thus, the selective intrabody interference with hAβO was able to normalize the microtubule instability to physiological control levels, by acting on endogenous murine Tau and tubulin (Fig. 25A, B). Of note, the immunofluorescence staining for the two forms of αtubulin and the Tau1/AT8 tau epitopes confirms the WB results (fig. 25C). As a consequence of the microtubule instability recover, Tg2576_A13K neurospheres gave rise to fully differentiated Tuj1+ positive neurons, whose degree of maturation, in terms of neurites length, was comparable to that of control neurons (Fig. 25C). In conclusion, I report the first evidence that morphological defects and cytoskeleton alterations of Tg2576 neurons derived from aNSCs are upstream driven by AβOs in a tau and tubulin dependent manner.

3.5 *In vivo* delivery of ScFvA13-KDEL intrabody rescues aNSCs proliferation and olfactory bulbs neurogenesis

To test the hypothesis whether endogenous AβOs were responsible for the proliferative and differentiative impairment of Tg2576 progenitors also *in vivo*, I performed intracerebral

delivery of pLentiA13K-GFP virus into the SVZ of 1.5 months old Tg2576 mice, through stereotactic injection. The intrabody expression in Tg2576 progenitors in the SVZ *in vivo* rescues their proliferation, in terms of BrdU incorporation and number of Sox2+ cells, while the number of Dcx+ neuroblasts was lower compared to that in non-infected Tg2576 mice (Fig. 26A-C). This latter result well correlates with an increase in the olfactory bulb neurogenesis, as demonstrated by a higher number of BrdU+/NeuN+ and BrdU+/Calretinin+ newborn neurons in the olfactory bulb (Fig. 26D-E).

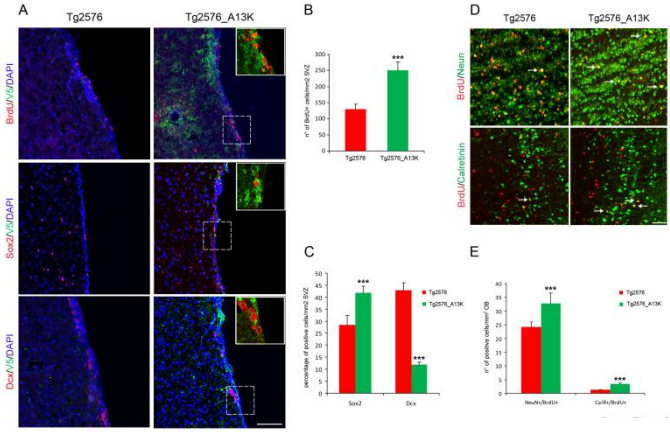

Figure 26. *In vivo* rescue of Tg2576 impaired neurogenesis by scFvA13K lentiviral infection.

A) Lentiviral delivery of scFvA13K intrabody to Tg2576 SVZ. The intrabody expression, confirmed by immunofluorescence staining for its c-terminal tag V5 (in green, right panels), leads to a significant rescue of proliferation, demonstrated by the increased number of BrdU+ cells (red signal), and restores the correct number of progenitors (Sox2+, red signal in middle right panel) and neuroblasts (Dcx+, red signal in bottom right panel) in the infected SVZ. DAPI staining on nuclei in blue. Scale bar 75µm, 40X magnification. White squared boxes in top panels represent 2.5X magnification of the corresponding dot-lines insets. B-C) Quantification of BrdU positive cells (B) and of Sox2 and Dcx positive cells (C) in Tg2576 (red) and Tg2576_A13K (green) SVZ. D-E) Immunostaining for BrdU and NeuN (red and green respectively, top panels,) and BrdU and Calretinin (red and green respectively, bottom panels) in the OB of

infected animals shows a significant increase of newborn CalR$^+$ interneurons derived from Tg2576_A13K SVZ progenitors compared to Tg2576, as quantified in the histogram (E). Scale bar 50µm, 40X magnification. Data are means ± SEM of five individual animals (n=5) for each experimental group. *** $p < 0.001$, significantly different from Tg2576, Student's t-test.

Ex-vivo analysis performed on primary neurospheres derived from infected and controlateral non-infected SVZ confirmed that the expression of scFvA13-KDEL persists also *in vitro* (Fig. 27A) and led to the same rescue, previously demonstrated *in vitro* by lentiviral infection, of both proliferation and differentiation defects of the SVZ progenitors (Fig. 27B-E). Thus, the intracellular interference with Aβ oligomers *in vivo*, through the delivery of scFvA13-KDEL intrabody, restores a correct adult SVZ neurogenesis.

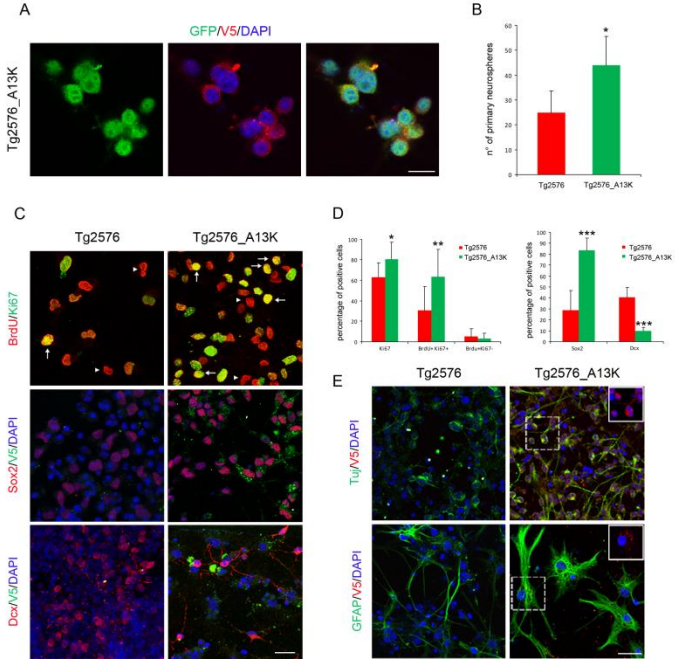

Figure 27. Ex vivo rescue of Tg2576 proliferative and differentiative defects by scFvA13 lentiviral infection.

A-C) aNSCs derived from infected SVZ (Tg2576_A13K) express both A13 intrabody (V5, red signal) and GFP (green signal). DAPI staining on nuclei in blue. Scale bar 10µm, 63X magnification, zoom 2. B) Quantification of the number of primary neurospheres derived from Tg2576 (red) and Tg2576_A13K (green) SVZ show ex-vivo rescue of proliferation by the *in vivo* intrabody expression. This was also confirmed by immunofluorescence staining for BrdU and Ki67 (red and green signals in C, respectively, in the top panels), showing more $BrdU^+$ (arrowheads) and double $BrdU^+/Ki67^+$ (arrows) cells in Tg2576_A13K samples compared to their non-infected counterpart, as quantified in D. C) The intrabody expression (V5 staining, green signal) in Sox2 and Dcx cells (red signal in middle and in bottom panels, respectively) restores the correct number of progenitors and neuroblasts in Tg2576_A13K neurospheres culture, as quantified in the histogram in D. DAPI staining on nuclei in blue. Scale bar 25µm, 63X magnification. Data are means $\pm$ SEM of five individual animals (n=5) for each experimental group. * $p<0.05$, ** $p < 0.01$, *** $p < 0.001$, significantly different from Tg2576, Student's t-test. E) Immunofluorescence staining for neurons (TuJ1, green signal in top panels) and astrocytes (GFAP, green signal in bottom panels). The expression of scFvA13 intrabody ($V5^+$ cells, red signal) leads to a partial rescue of both the neuronal arborization (top panel) and the dystrophic cellular shape of astrocytes (bottom panels). DAPI staining on nuclei in blue. Scale bar 25µm, 63X magnification, zoom 1.5. White square boxes represent only the V5 signal (in red) of the corresponding dot-lines insets.

In conclusion, our data demonstrated that impaired adult neurogenesis is an early event occurring in the SVZ neurogenic niche of young Tg2576 mice, prior to Aβ plaques deposition and overt neurodegeneration, but dependent on the intracellular generation and accumulation of toxic AβOs in the aNSCs.

3.6 Early alterations in hippocampal neurogenesis are rescued by the intracellular interference of Aβ oligomers by an inducible scFvA13-KDEL intrabody

It was recently demonstrated that in Tg2576 mice at 3 months of age there is an alteration of hippocampal neurogenesis (Unger *et al*, 2016). I thus wanted to verify if this phenotype was already present in younger animals (1.5-2 months old) and if it was dependent on the Aβ oligomers accumulation in DG-GP NSCs,

as occurring in the SVZ. Similarly to what observed in the SVZ, transgenic hAβ was already expressed in the DG region of young Tg2576 mice as early as 1.5 months of age, in both resident and tissue-derived nestin+ progenitors and Dcx+ neuroblasts (Fig. 28A and Fig. 29A).

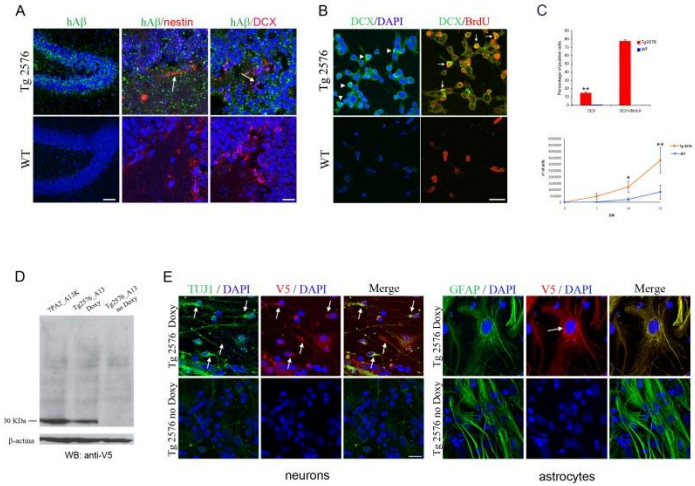

Figure 28. Rescue of neuronal differentiation of Tg2576 hippocampal progenitors by an inducible scFvA13_KDEL intrabody.

A) Aβ42 is highly expressed in resident DG-HP progenitors of Tg2576 mice. Double immunostaining for hAPP/Aβ (D54D2, green signal) and progenitors or neuroblasts/neuronal markers (red signal) in the dentate gyrus, showing hAPP/Aβ expression in both Nestin+ progenitors and Dcx+ neuroblasts in Tg2576 DG-HP but not in WT samples. DAPI staining on nuclei in blue. Scale bars 50µm, 40X magnification (left panels) and 20µm, 40X magnification, zoom 3 (central and right panels). B) Increase of Dcx+ neuroblasts in Tg2576 neurospheres. Double immunofluorescence for Dcx (green, arrowheads) and BrdU (red signal) shows the higher percentage of double positive proliferating cells (yellow, arrows) in Tg2576 neurospheres compared to WT, as quantified in the histogram in C (on the top). As consequence, Tg2576 hippocampal progenitors proliferate slightly more than WT cells (C, histogram on the bottom). DAPI staining on nuclei in blue. Scale bar 50µm, 63X magnification. D-E) Inducible scFvA13-KDEL intrabody rescues both neuronal and astrocytes differentiation of Tg2576 hippocampal progenitors. D) Western blot

analysis for V5 C-terminal tag showing that stable expression of scFvA13-KDEL intrabody is induced in Tg2576 neurospheres upon doxocycline (DOXO) administration, at levels comparable to those measured in control 7PA2 cells (Meli *et al*., 2014). E) Double immunofluorescence staining for Tuj1 or GFAP (green) and V5 tag (in red) showing that in DOXO-treated cells the expression of scFvA13-KDEL intrabody (arrows) increases neuronal maturation and arborization and partly restores the dystrophic shape of astrocytes. DAPI staining on nuclei in blue. Scale bars 25μm, 63X magnification, zoom 1.5 (neurons) and 10μm, 63X magnification, zoom 3 (astrocytes).

This was also confirmed by Western blot analysis for human APP and Aβ on neurospheres cell extracts and conditioned media, showing that only Tg2576 samples expressed high levels of full length APP, s-APP and Aβ monomers (Fig 29B), compared to WT. In agreement with the increased number of neuroblasts previously observed *in vivo* in this neurogenic niche (Unger *et al*, 2016), DG-derived Tg2576 neurospheres were also enriched in DCX neuroblasts (Tg2576 15%, WT 0.1%, $p<0.01$), actively proliferating, as demonstrated by the high percentage (approximately 80%) of BrdU/DCX double positive cells present in the neurospheres cultures (Fig. 28B-C). These subpopulation of Dcx+ neuroblasts was likely responsible of the increase in proliferation of Tg2576 neurospheres, compared to WT, Fig.28C). Despite that, Tg2576 Dcx+ cells failed to mature into TuJ1 positive neurons, as I found significantly less Tuj1+ neurons in Tg2576 than in WT samples (percentage of positive cells: Tg2576 2,5±0,2; WT 10,2±1,3, $p>0,01$) and with short neuritic processes, upon neurospheres differentiation (Fig. 29C-D). Also, GFAP+ cells displayed the same morphological alteration in their cell shape reported before in the SVZ-derived astrocytes (Fig. 29D, lower panels). These similarities in the aNSCs phenotype between the two neurogenic niches strongly suggested that the alteration in hippocampal neurogenesis might depend on the accumulation of intracellular Aβ oligomers, as I demonstrated for the SVZ. I thus expressed an inducible scFvA13-KDEL intrabody in Tg2576 hippocampal neurospheres through a tetracycline regulated lentiviral vector, pTRE_A13KDEL (see Materials and Methods for details). Upon

doxocyxline (DOXO) induction, the intrabody expression, revealed by Western blot analysis on neurospheres cell extracts against the V5 tag (Fig. 28C), restores proper neuronal and astrocytes differentiation (Fig. 29E and Fig. 28E).

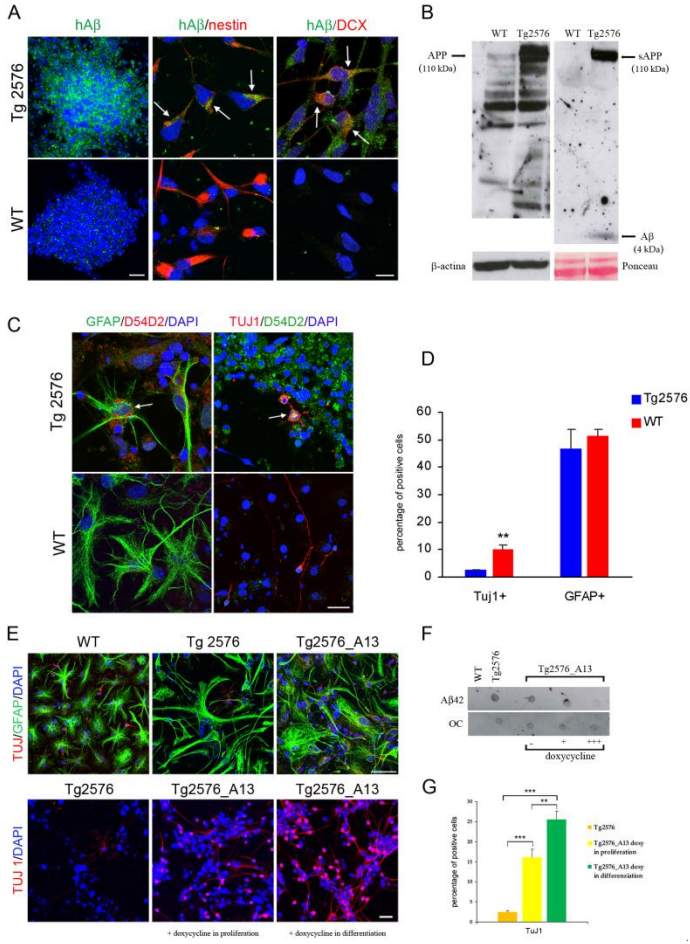

Figure 29. Early alterations in hippocampal neurogenesis are rescued by scFvA13_KDEL.

A-B) hAPP and hAβ are highly expressed in Tg2576 hippocampal neurospheres. A) Double immunostaining for APP/Aβ (green signal)

and progenitors or neuroblasts/neuronal markers (red signal) in primary neurospheres, showing hAPP/Aβ expression in both Nestin$^+$ progenitors and Dcx$^+$ neuroblasts. DAPI staining on nuclei in blue. Scale bar 25µm, 40X magnification (neurospheres) and 10µm, 63X magnification, zoom 3.5 (cells). B) Western blot analysis (anti-Aβ WO2) on Tg2576 (n=5) and WT (n=5) lysates (left panel) and conditioned media (right panel) showing that human APP, sAPP and $A\beta_{42}$ are almost exclusively detected in Tg2576 samples. Quantifications are obtained from densitometric values of bands and normalized for β-actin (cell lysates) or for one band of Ponceau (conditioned media). Data are mean ± SEM of 3 independent experiments. C) Double immunostaining for TuJ1/D54D2 (red and green signal, respectively) and GFAP/ D54D2 (green and red signal, respectively) shows that Tg2576 aNSCs express high level of Aβ (arrows) and fail to differentiate properly, as shown by the drastic reduction of neurites of TuJ1+ neurons and the dystrophic cell shape of GFAP+ astrocytes, compared to WT controls. Scale bar 25µm, 63X magnification. D) Quantification of percentage of positive (TuJ1$^+$ or GFAP$^+$) cells in Tg2576 (red, n=5) and WT (blue, n=5) samples is expressed as mean ± SEM of 3 independent experiments. ** $p< 0.01$ (for TuJ1$^+$ neurons), significantly different from WT, Student's t-test. E) scFvA13_KDEL rescues hippocampal Tg2576 aNSCs differentiation. Double immunostaining for TuJ1 (red) and GFAP (green) shows that scFvA13 intrabody expression in Tg2576 neurospheres restored proper both neurons and astrocytes morphology. Scale bar 25µm, 63X magnification. F) Dot Blot analysis on lysates shows that the stable expression of PTRE_scFvA13-KDEL intrabody reduces the amount of AβOs to levels comparable to those measured in WT samples in a dose-dependent manner, while other conformers do not change. H-G) Effect of AβOs interference at different stage of aNSCs maturation. ScFvA13-KDEL intrabody expression is more effective in restoring *in vitro* neurogenesis when induced in neural stem cells during differentiation rather than proliferation, as shown by the increased number of TuJ1+ neurons (G) and their higher degree of their arborization.

By using increasing concentrating of DOXO I could modulate the expression level of scFvA13-KDEL intrabody (not shown), and therefore its efficacy in intercepting intracellular AβOs was dose-dependent: indeed, the highest DOXO concentration led to a complete abolishment of Aβ42 in the infected neurospheres (Fig. 29D). Moreover, scFvA13-KDEL was more effective in

increasing neuronal differentiation of Tg2576 aNSCs, in terms of number of TuJ1+ cells and degree of maturation, when expressed during neurospheres differentiation rather than during proliferation.
In conclusion, our data demonstrated that impaired adult neurogenesis is an early event occurring in both neurogenic niches of young Tg2576 mice, prior to Aβ plaques deposition and neurodegeneration but dependent on the intracellular accumulation of Aβ oligomers in the aNSCs.

3.7 The intracellular interference of Aβ oligomers by scFvA13-KDEL intrabody rescues the proliferative and differentiative defects of AD patient-derived neural precursors

To evaluate the proliferative and differentiative properties of human neural progenitors I derived neural precursors (NPs) from two hiPSCs (human induced pluripotent stem cells) lines (Fig. 30A, see Materials and Methods for details), obtained from one healthy control (409B2) and one AD patient (APPE693Δ), respectively (Kondo *et al*., 2013). Control and AD NPs expressed neural stem cell markers, such as Sox2 and Nestin, indicating that the neural induction was correctly achieved in both samples (Fig. 30B). Interestingly, Sox2+ early neural progenitors were located in cluster, recalling the disposition and organization of neural stem cell in the neurogenic niches and in neurospheres. AD NPs proliferated significantly more than control precursors, as previously observed for Tg2576 hippocampal progenitors. In fact, double immunostaining for Ki67 and BrdU, 24 hours after BrdU pulse, demonstrated that the percentage of proliferating $Ki67^{+}$ $BrdU^{+}$ double positive cells was significantly higher in AD NPs respect to their counterpart. Moreover, neurons derived from the AD precursors displayed short neuritic processes, as shown by the immunofluorescence for Tuj1 (red signal in Fig. 31C), recalling the same differentiation impairment observed in Tg2576 neurons.

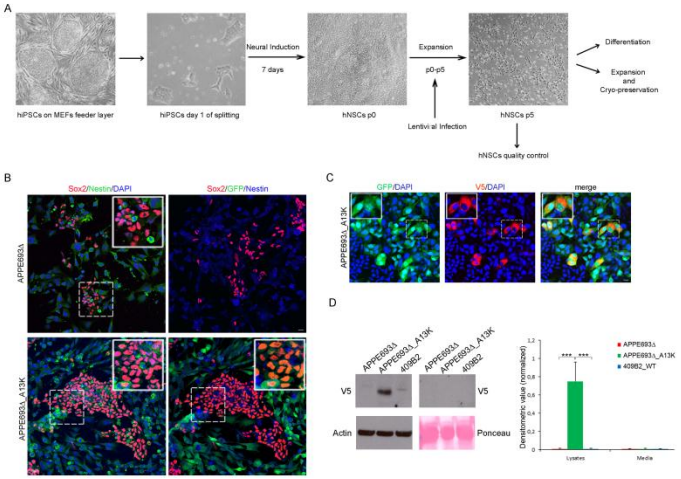

Figure 30. Derivation of human neural precursors and lentiviral delivery of scFvA13-KDEL.

A) Scheme of protocol for iPSCs conversion into human neural precursors (hNPs) (Y.Yaoung *et al*., 2013). B) Immunofluorescence staining for Sox2 and Nestin show that hiPSCs are properly converted into neural progenitors ($Sox2^+$ and $Nestin^+$ cells), while GFP expression indicates that this hNSCs are infected with the ScFvA13 lentiviral vector. DAPI staining on nuclei in blue. Scale bar 20µm, 40X magnification. Squared box is a 2X magnification of dots square box. C) APPE693Δ infected GFP^+ progenitors (APPE693Δ _A13K, green signal) stably express scFvA13-KDEL intrabody, as shown by immunofluorescence staining for its C-terminal V5 tag (red and merged signal). DAPI staining on nuclei in blue. Scale bar 20µm, 40X magnification. This is confirmed by western blot analysis of APPE693Δ, APPE693Δ_A13K and 409B2_WT cell lysates (left panel) and cell conditioned media (right panel) with antibodies against V5 tag. Quantifications are obtained from densitometric values of bands and normalized for β-actin (cell lysates) or for one band of Ponceau (conditioned media). Data are mean + SEM of 3 independent experiments. *** $p<0.001$, significantly different from APPE693Δ and 409B2_WT, Student's t-test.

To evaluate if both proliferation and differentiation defects were due to the Aβ oligomers accumulation in AD NPs, as occurring in the Tg2576 progenitors, I infected AD and control NPs with scFvA13_KDEL lentiviral vector. Stable expression of the intrabody was confirmed by GFP and V5 immunostaining (Fig. 30) and by Western blot analysis performed on cell lysates and conditioned media (Fig. 30D). Strikingly, scFvA13-KDEL intrabody rescued both the proliferative defects of AD NPs (Fig. 31A, B), and partially restored their neuronal maturation (Fig. 31C, central panel).

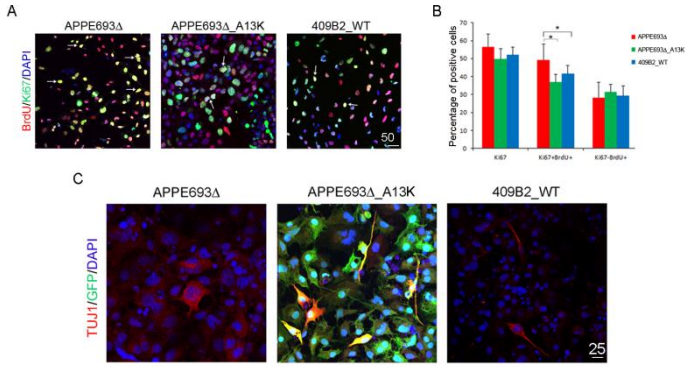

Figure 31. Stably expression of ScFvA13 rescues the APPE693Δ proliferative and differentiative impairment.
A-B) Double immunofluorescence for BrdU (red) and Ki67 (green) shows the rescue of the proliferative defect in AD NPs, decreasing the number of double positive proliferating cells (yellow arrowhead) in APPE693Δ_A13K NPs, as quantified in B. DAPI staining on nuclei in blue. Scale bar 50μm, 40X magnification. Data are mean + SEM of 3 independent experiments. *$p<0.05$, significantly different from APPE693Δ_A13K and 409B2_WT, Student's t-test. C) Immunostaining for TuJ1 (red) shows that APPE693Δ NSCs fail to differentiate properly, as shown by the reduction of neurites. Moreover the stable expression of ScFvA13_KDEL intrabody (GFP+ cells, central panel) rescues neuronal maturation and arborization. DAPI staining on nuclei in blue. Scale bar 25μm, 40X magnification.
.

3.8 ScFvA13 treatment rescues proliferative and differentiative defects of Tg2576 aNSCs

In order to investigate the effects of the interference with the extracellular Aβ oligomers on the proliferative and differentiative impairment of Tg2576 progenitors, I decided to provide scFvA13 to these cells as extracellularly administrated nanobody (Meli *et al*., 2009). ScFvA13 treatment rescued both the proliferative impairment and the differentiation defects of Tg2576 progenitors, as shown in Figure 32. In particular, scFvA13 increased the low number of both primary and secondary Tg2576 neurospheres at level comparable to WT (Fig.32A-B), in a dose-dependent manner. Furthermore, cell proliferation of Tg2576 treated with the lower nanobody concentration (0.2nM) was comparable to that of WT cells (Fig.32C). The positive effect of A13 on cell proliferation was restricted to Tg2576 progenitors, as WT cells did not increase their growth rate even at the highest nanobody concentration (2nM) (Fig.32A-B). This strongly suggested that the proliferative impairment of Tg2576 progenitors was due to extracellular accumulation of Aβ oligomers, intercepted by the addition of A13 in the culture medium. Indeed, WT progenitors treated with two different concentrations (10nM and 50nM) of human Aβ oligomers (hAβOs), or growth in Tg2576 neurospheres conditioned medium, showed a significant decrease in cell proliferation (Fig.19C). Western blot analysis showed that the nanobody C-terminal tag V5 is detectable only in the conditioned medium of Tg2576 A13-treated progenitors (Tg2576+0.2nM A13). The levels of extracellular free Aβ monomers increased in the CM of treated cells (Fig.32D), as consequence of the selective interference of ScFvA13 nanobody with the process of AβOs oligomerization (Meli *et al*, 2014).

Besides the effect on proliferation, both glial and neuronal morphology was correctly restored to WT phenotype by the nanobody treatment (Fig.32E-F). The effect of scFvA13 nanobody was more appreciable on astrocyte differentiation, which totally recovered the bushy-like morphology, typical of this cell type (Fig.32F).

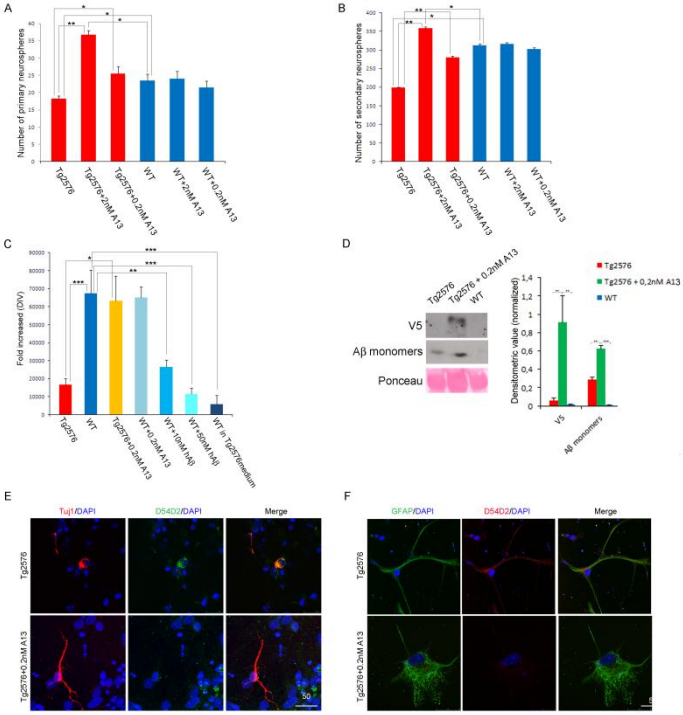

Figure 32. Extracellular administration of ScFvA13 to Tg2576 neurospheres rescues their proliferative and differentiative defects.

A-B) *In vivo* administration of ScFvA13 nanobody rescues the number of the primary and secondary (left and right histograms respectively) neurospheres to control values. Moreover, the nanobody treatment increases the proliferative rate of Tg2576 A13 in a dose-dependent manner (0.2nM and 2mM, respectively). Conversely, WT neurospheres treated with increasing concentrations of hAβ oligomers as shown in C. Data are mean + SEM of 3 independent experiments. * $p<0.05$, ** $p<0.01$ and ***$p<0.001$, significantly different from WT, Student's t-test. D) Western blot for Aβ peptides (WO2) in Tg2576, WT and Tg2576 + 0.2nM A13 conditioned media indicates that the nanobody increases the amount of free Aβ monomers in the treated sample. Moreover, western blot for nanobody C-terminal V5 tag demonstrated that the nanobody is accumulated only in treated

neurospheres medium, as quantified by the densitometric values reported in the corresponding histograms on the right, normalized for β-actin (for lysates) or Ponceau (for conditioned media). Data are mean + SEM of 3 independent experiments. * $p<0.05$, ** $p<0.01$ and ***$p<0.001$ significantly different from Tg2576 and WT, Student's t-test .E-F) Immunofluorescence staining for TuJ1 (red, E) and GFAP (green, F) shows that in Tg2576 + 0.2nM A13 sample the extracellular administration of scFvA13 nanobody leads to a rescue of both neuronal maturation and arborization and of the dystrophic shape of astrocytes. In addition, the treatment leads to a reduction of Aβ in both differentiated cell types. DAPI staining on nuclei in blue. Scale bar 50μm, 63X magnification.

3.9 The proliferative defect of APPE693Δ NPs is rescued by ScFvA13 extracellular treatment

I then wanted to extend our study on the interference of the extracellular AβOs also in human NPs. To this aim I treated AD NPs with 0.2nM scFvA13 nanobody every single day (following the same experimental conditions previously established with the Tg2576 progenitors). The scFvA13 nanobody was detectable only in conditioned medium derived from AD neural precursors treated for five days (APPE693Δ +0.2nMA13) (Fig. 33A-B). Notably, the nanobody treatment restored the proliferative rate of AD NPs at level comparable to that measured in 409B2_WT sample, as demonstrated by double immunofluorescence for Ki67 and BrdU (green and red signal respectively, Fig. 33C) and quantified in the histogram (Fig. 33D).

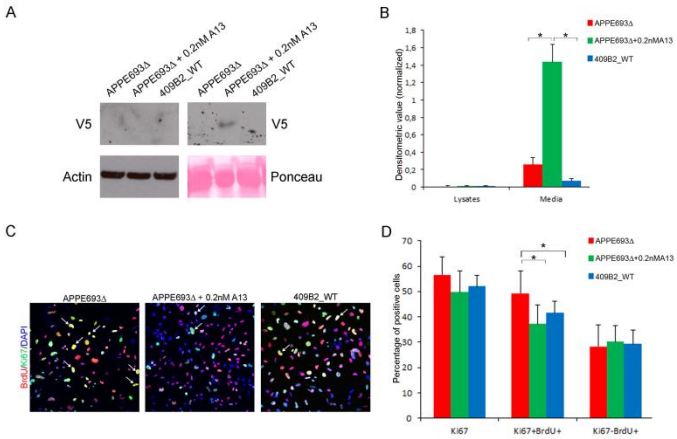

Figure 33. Extracellular administration of ScFvA13 to APPE693Δ NPs rescues their proliferative and differentiative defects.
A-B) Double immunofluorescence for BrdU (red signal) and Ki67 (green) shows that the *in vitro* administration of ScFvA13 nanobody rescues the APPE693Δ NSPs proliferative defect, as indicated by the reduction of double positive proliferating cells (yellow, arrowhead) in APPE693Δ + 0.2nM A13K sample and as quantified in B. DAPI staining on nuclei in blue, 40X magnification, scale bar 50µm. Data are mean + SEM of 3 independent experiments. * $p<0.05$, significantly different from APPE693Δ+0.2nM A13 and 409B2_WT, Student's t-test. C-D) Western blot analysis of APPE693Δ, APPE693Δ+0.2nM A13 and 409B2_WT cell lysates and conditioned media with antibody against the ScFvA13 nanobody C-terminal tag V5 demonstrated that ScFvA13 nanobody is accumulated only in treated hNPs medium, as quantified by the densitometric values reported in the histogram (D), normalized for β-actin (for lysates) or Ponceau (for conditioned media). Data are mean + SEM of 3 independent experiments. * $p<0.05$, significantly different from APPE693Δ and 409B2_WT, Student's t-test.

In conclusion, the interference with the extracellular hAβ oligomers by the scFvA13 intrabody is effective also in human, AD-derived neural precursors.

4.Discussion

In this work I demonstrated that impairment of adult neurogenesis, mediated by Aβ oligomers, is an early event in Alzheimer's disease pathogenesis. Indeed I provided evidence of a causal link between the intracellular accumulation of endogenous oligomeric Aβ in aNSCs and altered neurogenesis, involving tau-dependent mechanism(s) and occurring prior to neurodegeneration. Until now, very little was known about alterations in neurogenesis at the beginning of the disease or before the onset of amyloid-plaque formation. By performing my analysis in young Tg2576 transgenic mice, a well-characterized animal model for AD, at 1.5-2 month of age, that is considered pre-symptomatic in terms of Aβ plaques formation and neurodegeneration (Kim *et al*., 2012), I unraveled a major defect in neurogenesis, occurring before any the appearance of the neuropathology alterations. This deficit in adult neurogenesis well correlates with the accumulation of endogenous, natural-occurring Aβ oligomers (AβOs) in the neural stem cells derived from both the SVZ and the DG-HP neurogenic niches. An independent study shows a defect on dentate gyrus neurogenesis in 3 months old Tg2576 correlated with the presence of thioflavin S staining (Unger *et al*., 2016) but without any characterization of the Aβ/AβOs biochemical profiles. Here I demonstrated the presence of considerable amount of Aβ peptides at 1.5-2 months, both on histological SVZ and DG_HP brain sections and in neural stem cells derived from these neurogenic niches. By exploring the Tg2576 neurosphere cultures, I provided a detailed biochemical profile of the different intracellular Aβ species present in AD adult neural stem cells, and thus I demonstrated for the first time that intracellular AβOs are generated in adult aNSCs and are responsible for both the proliferative impairment and the neurogenic defects of these cells, as well as for the morphological defects of neurons and astrocytes. The causal role of intracellular AβOs in determining the neurogenesis defects has been formally demonstrated by the intracellular interception of AβOs by the scFvA13 intrabody in aNSCs, which was able to reestablish proper neuronal and glial differentiation. To my knowledge, this is the first evidence that formally demonstrates that intracellular Aβ oligomers play a

specific role in modulating both proliferation and differentiation of NSC. In fact, previous studies either did not discriminate accurately between the different Aβ species, due to the use of anti-Aβ antibodies that recognize several Aβ/APP isoforms (4G8, 6E10), or used synthetic, rather than natural occurring, $A\beta_{42}$ peptides (Diaz-Moreno *et al*., 2013). Instead, scFvA13KDEL intrabody specifically intercepts endogenous biologically-active AβOs conformers (Meli *et al*., 2009; Meli *et al*., 2014) and lead to their functional silencing, both *in vitro* and, notably, *in vivo*. In fact, I demonstrated here that scFvA13 intrabody expression in Tg2576 SVZ rescues olfactory bulbs neurogenesis and restores SVZ-derived aNSCs proliferation and differentiation. In addition, the use of an inducible lentiviral vector to deliver scFvA13-KDEL intrabody in the hippocampal progenitors allowed us to time-modulate its expression and thus to reveal the right developmental window in which intercept the AβOs for a better restoration of adult neurogenesis. The relevance of this finding is dual, as i) it demonstrates that an intracellular accumulation of AβOs occurs in neural stem cells and affect adult neurogenesis long before the onset of neurodegeneration, and ii) it would be of benefit in the development of new strategies aimed to restore or reinforce adult neurogenesis as a complementary therapeutic interventions for AD disease. Moreover, my results validate adult neurogenesis as an early pre-symptomatic alteration in the neurodegeneration progression and prospect targeting intracellular Aβ oligomers as a therapeutic strategy to be pursued.

Despite the majority of Tg2576 progenitors give rise to Tuj1+ cells, *in vitro* neuronal differentiation is greatly impaired. This result confirmed what already observed *in vivo* in Tg256 SVZ here, where I found more Dcx+ neuroblasts that nevertheless fail to execute a functional neurogenesis. Calafiore and colleagues (2006) demonstrated that $A\beta_{1\text{-}42}$ drives NSCs of the SVZ towards a neural lineage. My results confirmed this data showing that this orientation towards the neural lineage is indeed accompanied by a lower degree of maturation of Tg2576 neurons that present a shorter axon than their control counterpart. This is in accordance with Waldau and Shetty

(2008), who demonstrated that the accumulation of toxic $A\beta_{1-42}$ oligomers in AD brains first stimulated the differentiation of NPCs into SGZ, but later, when such oligomers turn into fibrillary plaques, the newly formed neuroblasts could not complete their maturation process. The same happened also in my Tg2576 hippocampal neurospheres, which failed to differentiate into mature neurons despite their enrichment in Dcx+ neuroblasts.

In addition to the neurogenic defects, I also found a severe morphological alteration of astrocytes, as shown by the atypical elongated shape of GFAP+ cells present both *in vitro* in the differentiating Tg2576 neurospheres and *in vivo* in the SVZ. This phenotype is reminiscent of similar *in vivo* observations in animal models for AD (Rodriguez *et al*., 2009; Perez *et al*., 2010) and might be related to neurotoxic reactive A1 astrocyte phenotype (Liddelow *et al*., 2017). Alterations in the glial compartment, linked either to atrophy or to astrogliosis are observed in different phases of the AD neurodegenerative process. It is worth noting that both aggregated Aβ protein, the intact cores of Aβ plaques and Aβ fragments stimulated the astrogliosis. This process is accompanied by the presence of reactive astrocytes, which are characterized by alteration in their cell shape, similar to those present in the Tg2576 astrocytes. Here I demonstrate for the first time that the morphological defects observed in Tg2576 neurons and astrocytes are likely due to cytoskeleton abnormalities, tau-mediated, already present in the neural stem cells compartment. Indeed, Tg2576 neurospheres display hyperstabilized, pathologically less dynamic microtubules, as indicated by the dramatic tau dephosphorylation and the important up-regulation in acetyl Tub-positive microtubules. The depletion of intracellular soluble Aβ oligomers is actually able to revert these events, normalizing both the site-specific phosphorylation at Tau1/AT8 epitopes (Ser198/Ser202//pThr205). As a consequence, correct neurons and astrocytes cell morphology is restored. These results are in agreement with previous findings reporting the Aβ-dependent decreased microtubule dynamics via tubulin hyperacetylation (Tsushima *et al*., 2015) and a marked tau site-specific dephosphorylation with pathological

microtubule hyperstabilization (Golovyashkina *et al*., 2015), both *in vitro* and *ex-vivo* in AD neuronal models.
As a further contribution to this field I provide evidence that i) the pathological, tau-mediated, microtubule hyperstabilization in neural stem cells is responsible for morphological alterations occurring during differentiation; ii) this phenomenon is driven by intracellular Aβ oligomers accumulation, as their interception by the scFvA13 reestablishes proper neuronal and glial differentiation, through the normalization of tau phosphorylation.
Comparable results were obtained in human NPs that stably expressed the ScFvA13 intrabody.
Altogether, the relevance of my findings is manifold, as it demonstrates that: i) the generation of toxic/bioactive AβOs occurs intracellularly in neural stem cells; ii) this pool of AβOs, targeted with a selective intrabody intereference, affects adult neurogenesis long before the onset of overt neurodegeneration; iii) a new mechanism of microtubule destabilization driven by human AβOs and acting on endogenous murine tau and tubulin. Thus, strategies aimed at restoring or reinforcing adult neurogenesis might be highly relevant, as complementary or alternative therapeutic interventions for AD disease. In this respect, the demonstration that the action of AβOs in inducing alterations in SVZ neurogenesis is cell autonomous provides additional new evidence to the concept of intracellular AβOs as a key target (Forloni *et al*., 2018; Ono, 2017; Meli *et al*., 2014), thus prospecting targeting intracellular Aβ oligomers in neurogenic niches as a therapeutic strategy to be explored further.
Indeed, my results prospects adult neurogenesis as an early pre-symptomatic alteration in the neurodegeneration progression in this well-established AD model. Certainly, these results shed new light on the possible interpretation regarding the role of altered neurogenesis in AD: a key event occurring before the onset of the disease, or participating at early stage to the pathology progression. This prompts to investigate systematically whether adult neurogenesis markers in the neurogenic niches represent an early biomarker also in human AD brains. In this respect, it is noteworthy that markers for

adult neurogenesis in the human CSF are being described (Lugert *et al*., 2017), and could serve as proxies for the rates of neurogenesis in the brain. A CSF biomarker reflecting the extent of early alterations of neurogenesis in MCI or in non-demented patients with memory loss would be extremely valuable for longitudinal studies, for early diagnosis and patient stratification, or for monitoring treatment efficacy.

In addition, I demonstrated that also extracellular AβOs played an important role in controlling both proliferation and differentiation of NSC. In fact, extracellular AβOs silencing by ScFvA13 nanobody treatment leads to a significant rescue of the proliferative impairment in Tg2576 NSCs as well as of their neurogenic defects. Interestingly, the nanobody effect on proliferative impairment is dose-dependent. Of note, one of the most striking effects of the nanobody treatment is the rescue of the altered cell shape of AD astrocytes, which completely recover their typical bush-like morphology. This can be probably explained by one of critical role played by astrocytes in AD neurodegeneration is the clearance of the extracellular environment in the nervous system. Thus, by silencing AβOs, we can assume that nanobody treatment might alleviate the cellular damage occurring during internalization and degradation of these neurotoxic Aβ species (Wyss-Coray *et al*., 2003; Funato *et al*., 1998; Thal *et al*., 1999). Similar ScFvA13 nanobody effect are demonstrated on human-AD NPs about the proliferative impairment, further emphasizing both the AβOs role in the alteration of adult neurogenesis in Alzheimer's disease and the amazing ability of the ScFvA13 nanobody to restore physiological neurogenesis.

Altogether, these data demonstrate for the first time that Aβ oligomers affect both proliferation and differentiation of adult aNSCs long before the onset of AD neurodegeneration. I also demonstrated the potential efficacy of targeting intracellular AβOs in aNSCs as a therapeutic strategy to rescue the neurogenesis defect and validated the scFvA13 intrabody as a new selective, therapeutic tool, able to neutralize intracellular natural-occurring AβOs and, at the same time, to restore a functional neurogenesis.

5. Conclusions

In summary, this thesis demonstrates for the first time that impaired adult neurogenesis is an early event occurring in both neurogenic niches of young Tg2576 mice, prior to Aβ plaques deposition and neurodegeneration but dependent on the intracellular accumulation of Aβ oligomers in the aNSCs.

In particular, by analyzing the proliferative and differentiative features of Tg2576 aNSCs I demonstrated that these cells proliferate significantly less, with respect to their control counterparts. Tg2576 neurospheres derived from the SVZ niche are enriched in DCX^+ neuroblasts, which failed to terminally differentiate, and give rise to less GFAP+ astrocytes, with an aberrant morphology. These defects have been confirmed also *in vivo*, where a defective olfactory bulbs neurogenesis is observed.

Reduced proliferation and differentiation impairment of Tg2576 progenitors *in vitro* are caused by endogenous oligomeric Aβ (AβOs): indeed, both defects were rescued by the expression of a conformation-specific intrabody, scFvA13-KDEL, which selectively interferes with the early intracellular generation of AβOs. Noteworthy, scFvA13-KDEL intrabody restores also the pathological microtubule hyperstabilization of newly formed neurons, which is tau-mediated. To our knowledge, this is the first formal demonstration of a new mechanism of microtubule destabilization driven by human AβOs and acting on endogenous murine tau and tubulin.

Finally, lentiviral-mediated *in vivo* expression of the intrabody in Tg2576 SVZ rescues the olfactory bulbs neurogenesis, and restores SVZ-derived aNSCs proliferation and differentiation.

Early alterations in adult neurogenesis were also present in the other neurogenic niche of Tg2576 mice, the dentate gyrus of the hippocampus (DG-HP). Similarly to the SVZ-derived progenitors, hippocampal progenitors displayed high amount of intracellular Aβ oligomers and undergo neuronal and astrocytic differentiation impairment. Both defects were rescued by the AβOs intracellular targeting with an inducible scFvA13-KDEL intrabody.

Furthermore, I demonstrated that also extracellular AβOs played an important role in controlling both proliferation and differentiation of aNSCs. In fact, the extracellular

administration of ScFvA13 nanobody to Tg2576 aNSCs significantly rescues their proliferative impairment as well as their neurogenic defects, in a dose-dependent manner. Strikingly, I demonstrated the efficacy of ScFvA13KDEL, both as intrabody and nanobody, in restoring AβOs-dependent proliferative and differentiative impairment also in human-AD NPs.

Altogether, our results demonstrate that impaired neurogenesis is an early event, occurring at a presymptomatic age prior to overt neurodegeneration and is caused by endogenous AβOs accumulation in the neurogenic niches. Notably, the intra- or extracellular interception of AβOs by scFvA13 intrabody in aNSCs reestablishes proper neuronal and glial differentiation. This important finding demonstrates the potential efficacy of targeting intracellular AβOs in aNSCs as a therapeutic strategy to restrain neuronal degeneration in AD.

The results hereby presented leave some unsolved questions. For instance, it remains to be seen whether and how rescuing the early neurogenesis defect in Tg2576, by intercepting intracellular AβOs in the neurogenic niche(s), is able to provide a more general protection on the progress of neurodegeneration in the affected brains. In addition, the potential efficacy of scFvA13 antibody in targeting and neutralize intracellular natural-occurring AβOs in aNSCs, and thus restore a functional neurogenesis, has not been tested in experimental model for sporadic AD, such as patients-derived iPSCs and iNs (induced neurons). Also, the more effective and less invasive antibody delivery, either as intrabody or nanobody, remains to be assessed. This will be of extreme interest, as it will validate the scFvA13 antibody as a new selective, therapeutic tool, to be exploited in alternative curative approaches for AD.

6. Acknowledgements

First of all, I would like to thank my family, who supported every choice I made, coping with all consequences, standing always on my side and always believing in me. Specifically, I have to thank my parents who showed me that love and commitment always pay off.

Thanks to my sweetheart, my other half, who shared with me all my doubts and fears, as well as the excitement and happiness when my experiments succeeded. Again, thank you Marco, for believing in my skills, sometimes overrating me, and for always calming me down and for loving me. My sweet Tilla deserves another "thanks", as for sometimes she had to share her mom with a laptop and this thesis. As always, she cheers me up with her smile and her cries.

Only thanking my Boss, instead, is not enough. An extraordinary woman, much more than a supervisor to me. I can easily say that everything I learnt, I learnt it from her. I feel I am super lucky to have her as a guide. She's always pushed and encouraged me so that I could do better. She's the one I can always talk to for working issues and, most importantly, a friend outside the lab.

I also would like to thank Silvia and Alessia, women of my life, who I am always sharing every single moment with.

Thanks to my colleagues who I spent the latest three years and drank tons of coffee with. Particularly, I want to thank Vero and Fede, who prove themselves to be real friends. The former always happy to help, despite having little time, and the latter who has always been able to calm my worrying, before from sitting next to me and now from far away.

Thanks to Donatella and Adriana, who despite the distances and different paths, are always there for me.

Thanks to Marianna, Geppy, Dano, Maier, Gian and Sandro, who I met 8 years ago and with whom I shared happiness and

university anxieties and whom I am still keeping in my heart, despite we don't meet so often anymore.

Thanks to Giulia, simply (so to speak) a great friend.

And, last but not at least, thanks to Professor Sandra Moreno, who has always advised and addressed me in the thesis's work.

Finally, thanks to all my friends and colleagues who gave me a smile, making my job and life better.

7.References

Amlien IK, Fjell AM. Diffusion tensor imaging of white matter degeneration in Alzheimer's disease and mild cognitive impairment. *Neuroscience*, 2014; S0306-4522(14)00121-3.

Ballard C, Gauthier S, Corbett A, Brayne C, Aarsland D, Jones E. Alzheimer's disease. *Lancet*, 2011; 377:1019-31.

Bergmann O., Spalding KL., and Frisén J. Adult Neurogenesis in Humans. *Cold Spring Harb Perspect Biol*, 2015; 7:a018994

Bergmann, O., Liebl, J., Bernard, S., Alkass, K., Yeung, M.S., Steier, P., Kutschera, W., Johnson, L., Lande´ n, M., Druid H, Spalding KL, Frisén J. The age of olfactory bulb neurons in humans. *Neuron*, 2012; 74(4):634-9

Bilkei-Gorzo A. Genetic mouse models of brain ageing and Alzheimer's disease. *Pharmacol Ther*, 2014; 142:244-57.

Bonds JA, Kuttner-Hirshler Y, Bartolotti N, Tobin MK, Pizzi M, Marr R, Lazarov O. Presenilin-1 Dependent Neurogenesis Regulates Hippocampal Learning and Memory. *PLoS One*, 2015; 10(6): e0131266.

Calafiore M, Battaglia G, Zappala A, Trovato-Salinaro E, Caraci F, Caruso M, Vancheri C, Sortino MA, Nicoletti F, Copani A. Progenitor cells from the adult mouse brain acquire a neuronal phenotype in response to beta-amyloid. *Neurobiol Aging*, 2006; 27(4): 606-613.

Ciammola A, Sassone J, Cannella M, Calza S, Poletti B, Frati L, Squitieri F, Silani V. Low brain-derived neurotrophic factor (BDNF) levels in serum of Huntington's disease patients. Am J Med Genet B *Neuropsychiatr Genet*, 2007; 144B:574-7.

Conde C, Caceres A. Microtubule assembly, organization and dynamics in axons and dendrites. *Nat Rev Neurosci*, 2009; 10(5): 319-332.

Conforti P, Ramos C, Apostol BL, Simmons DA, Nguyen HP, Riess O, Thompson LM, Zuccato C, Cattaneo E. Blood level of brain-derived neurotrophic factor mRNA is progressively reduced in rodent models of Huntington's disease: restoration by the neuroprotective compound CEP-1347. *Mol Cell Neurosci*, 2008; 39:1-7.

Conti L, Cattaneo E. Neural stem cell systems: physiological players or *in vitro* entities? *Nat Rev Neurosci*, 2010;11:176-87.

D'Amelio M, Cavallucci V, Middei S, Marchetti C, Pacioni S, Ferri A, Diamantini A, De Zio D, Carrara P, Battistini L, Moreno S, Bacci A, Ammassari-Teule M, Marie H, Cecconi F. Caspase-3 triggers early synaptic dysfunction in a mouse model of Alzheimer's disease. *Nat Neurosci*, 2011; 14:69-76.

Dayer AG, Cleaver KM, Abouantoun T, Cameron HA. New GABAergic interneurons in the adult neocortex and striatum are generated from different precursors. *J Cell Biol*, 2005;168: 415–427.

Diaz-Moreno M, Hortiguela R, Goncalves A, Garcia-Carpio I, Manich G, Garcia-Bermudez E, Moreno-Estellès M, Eguiluz V, Vilaplana J, Pelegrì C, Vilar M, Mira H. Abeta increases neural stem cell activity in senescence-accelerated SAMP8 mice. *Neurobiol Aging*, 2013; 34(11): 2623-2638.

Ernst A, Frisen J. Adult neurogenesis in humans- common and unique traits in mammals. *PLoS Biol*, 2015; **13**(1)**:** e1002045.

Ernst A, Alkass K, Bernard S, Salehpour M, Perl S, Tisdale J, Possnert G, Druid H, Frisén J. Neurogenesis in the striatum of the adult human brain. *Cell*, 2014 ;156(5):1072-83

Forloni G, Balducci C. Alzheimer's Disease, Oligomers, and Inflammation. *J Alzheimers Di,s* 2018; 62(3): 1261-1276.

Frielingsdorf H, Schwarz K, Brundin P, Mohapel P. No evidence for new dopaminergic neurons in the adult mammalian substantia nigra. *Proc Natl Acad Sci U S A*, 2004; 101:10177-82.

Funato H, Yoshimura M, Yamazaki T, Saido TC, Ito Y, Yokofujita J, Okeda R, Ihara Y. Astrocytes containing amyloid beta-protein (Abeta)-positive granules are associated with Abeta40-positive diffuse plaques in the aged human brain. *Am J Pathol*. 1998; 152(4):983-92.

Goedert M. Parkinson's disease and other alpha-synucleinopathies. *Clin Chem Lab Med*, 2001; 39:308-12.

Golovyashkina N, Penazzi L, Ballatore C, Smith AB, 3rd, Bakota L, Brandt R. Region-specific dendritic simplification induced by Abeta, mediated by tau via dysregulation of microtubule dynamics: a mechanistic distinct event from other neurodegenerative processes. *Mol Neurodegener*, 2015; 10: 60.

Gritti A, Frölichsthal-Schoeller P, Galli R, Parati EA, Cova L, Pagano SF, Bjornson CR, vescovi AL. Epidermal and fibroblast growth factors behave as mitogenic regulators for a single multipotent stem cell-like population from the subventricular region of the adult mouse forebrain. J *Neurosci*, 1999;19:3287-97.

Hardy J, Selkoe DJ. The amyloid hypothesis of Alzheimer's disease: progress and problems on the road to therapeutics. Science, 2002; 297:353-356.

Haughey N. J, Nath A, Liu D, Chan S. L, Borchard A. C, Rao M. S, and Mattson M. P. Disruption of neurogenesis by amyloid β-peptide and perturbed calcium homeostasis in models of Alzheimer's disease. J. Neurosci, 2002a; 83:1509-24.

Haughey NJ, Liu D, Nath A, Borchard AC, Mattson MP. Disruption of neurogenesis in the subventricular zone of

adult mice, and in human cortical neuronal precursor cells in culture, by amyloid beta-peptide: implications for the pathogenesis of Alzheimer's disease. *Neuromolecular Med*, 2002b; 1:125-35.

Haughey NJ, Nath A, Chan SL, Borchard AC, Rao MS, Mattson MP. Disruption of neurogenesis by amyloid beta-peptide, and perturbed neural progenitor cell homeostasis, in models of Alzheimer's disease. *J Neurochem*, 2002; 83(6): 1509-1524.

Heo C, Chang KA, Choi HS, Kim HS, Kim S, Liew H, Kim JA, Yu E, Ma J, SuhYH. Effects of the monomeric, oligomeric, and fibrillar Abeta42 peptides on the proliferation and differentiation of adult neural stem cells from subventricular zone. *J Neurochem*, 2007; 102(2): 493-500.

Hodge RD, Kahoud RJ, Hevner RF. Transcriptional control of glutamatergic differentiation during adult neurogenesis. *Cell Mol Life Sci*, 2012; 69:2125-34.

Höglinger GU, Rizk P, Muriel MP, Duyckaerts C, Oertel WH, Caille I, Hirsch EC. Dopamine depletion impairs precursor cell proliferation in Parkinson disease. *Nat Neurosci*, 2004; 7:726-35.

Hollands C, Tobin MK, Hsu M, Musaraca K, Yu TS, Mishra R, Kernie SG, Lazarov O. Depletion of adult neurogenesis exacerbates cognitive deficits in Alzheimer's disease by compromising hippocampal inhibition. *Mol Neurodegener*, 2017; 12(1): 64.

Holtzman DM, Mandelkow E, Selkoe DJ. Alzheimer disease in 2020. *Cold Spring Harbor Perspect Med*, 2012; 2.

Hsiao K, Chapman P, Nilsen S, Eckman C, Harigaya Y, Younkin S, Yang F, Cole G. Correlative memory deficits, Abeta elevation, and amyloid plaques in transgenic mice. *Science*, 1996; 274(5284): 99-102.

Imayoshi I, Sakamoto M, Ohtsuka T, Takao K, Miyakawa T, Yamaguchi M, Mori K, Ikeda T, Itohara S, Kageyama R. Roles of continuous neurogenesis in the structural and functional integrity of the adult forebrain. *Nat Neurosci*, 2008; 11:1153-61.

Inta D, Alfonso J, von Engelhardt J, Kreuzberg MM, Meyer AH, van Hooft JA, Monyer H. Neurogenesis and widespread forebrain migration of distinct GABAergic neurons from the postnatal subventricular zone. *Proc Natl Acad Sci*, 2008; 105: 20994–20999.

Iqbal K, Liu F, Gong CX. Alzheimer disease therapeutics: Focus on the disease and not just plaques and tangles. *Biochem Pharmacol*, 2014; 88:631-639.

Irizarry MC, McNamara M, Fedorchak K, Hsiao K, Hyman BT. APPSw transgenic mice develop age-related A beta deposits and neuropil abnormalities, but no neuronal loss in CA1. *J Neuropathol Exp Neurol,. 1997;*56*(9):965-7.*

Jacobsen JS, Wu CC, Redwine JM, Comery TA, Arias R, Bowlby M, Martone R, Morrison JH, Pangalos MN, Reinhart PH, Bloom FE. Early-onset behavioral and synaptic deficits in a mouse model of Alzheimer's disease. *Proc Natl Acad Sci U S A*, 2006; 103:5161-6.

Janning D, Igaev M, Sundermann F, Bruhmann J, Beutel O, Heinisch JJ, Bakota L, Piehler J, Junge W, Brandt R. Single-molecule tracking of tau reveals fast kiss-and-hop interaction with microtubules in living neurons. *Mol Biol Cell*, 2014; 25(22): 3541-3551.

Jin K, Peel AL, Mao XO, Xie L, Cottrell BA, Henshall DC, Greenberg DA. Increased hippocampal neurogenesis in Alzheimer's disease. *Proc Natl Acad Sci U S A*, 2004; 101:343–347.

Johnson GV, Stoothoff WH. Tau phosphorylation in neuronal cell function and dysfunction. *J Cell Sci*, 2004; 117(Pt 24): 5721-5729.

Kim TK, Lee JE, Park SK, Lee KW, Seo JS, Im JY, Kim ST, Lee JY, Kim YH, Lee JK, Han PL. Analysis of differential plaque depositions in the brains of Tg2576 and Tg-APPswe/PS1dE9 transgenic mouse models of Alzheimer disease. *Exp Mol Med*, 2012; 44(8): 492-502.

King DL, Arendash GW. Behavioral characterization of the Tg2576 transgenic model of Alzheimer's disease through 19 months. *Physiol Behav*, 2002; 75:627-42.

Lazic SE, Grote H, Armstrong RJ, Blakemore C, Hannan AJ, van Dellen A, Barker RA. Decreased hippocampal cell proliferation in R6/1 Huntington's mice. *Neuroreport*, 2004;15:811-3.

Lee IS, Jung K, Kim IS, Park KI. Amyloid-β oligomers regulate the properties of human neural stem cells through GSK-3β signaling. *Exp Mol Med*, 2013;45:e60.

Lemere CA. Immunotherapy for Alzheimer's disease: hoops and hurdles. *Mol Neurodegener*, 2013; 8:36.

Li QX, Maynard C, Cappai R, McLean CA, Cherny RA, Lynch T, Culvenor JG, Trevaskis J, Tanner JE, Bailey KA, Czech C, Bush AI, Beyreuther K, Masters CL. Intracellular accumulation of detergent-soluble amyloidogenic A beta fragment of Alzheimer's disease precursor protein in the hippocampus of aged transgenic mice. *J Neurochem*, 1999; 72:2479-87

Li SH1, Li XJ. Huntingtin-protein interactions and the pathogenesis of Huntington's disease. *Trends Genet*, 2004; 20:146-54.

Liddelow SA, Guttenplan KA, Clarke LE, Bennett FC, Bohlen CJ, Schirmer L, Bennett ML, Münch AE, Chung WS, Peterson TC, Wilton DK, Frouin A, Napier

BA, Panicker N, Kumar M, Buckwalter MS, Rowitch DH, Dawson VL, Dawson TM, Stevens B, Barres BA. Neurotoxic reactive astrocytes are induced by activated microglia. *Nature*, 2017; 541(7638): 481-487.

Lie DC, Dziewczapolski G, Willhoite AR, Kaspar BK, Shults CW, Gage FH. The adult substantia nigra contains progenitor cells with neurogenic potential. *J Neurosci*, 2002; 22:6639-49.

Lopez-Toledano MA, Shelanski ML. Neurogenic effect of beta-amyloid peptide in the development of neural stem cells. *J Neurosci*, 2004; 24(23): 5439-5444.

Lugert S, Kremer T, Jagasia R, Herrmann A, Aigner S, Giachino C, Mendez-David I, Gardier AM, Carralot JP, Meistermann H, Augustin A, Saxe MD, Lamerz J, Duran-Pacheco G, Ducret A, Taylor V, David DJ, Czech C. Glypican-2 levels in cerebrospinal fluid predict the status of adult hippocampal neurogenesis. *Sci Rep*, 2017; 7: 46543.

Meli G, Lecci A, Manca A, Krako N, Albertini V, Benussi L, Ghidoni R, Cattaneo A. Conformational targeting of intracellular Abeta oligomers demonstrates their pathological oligomerization inside the endoplasmic reticulum. *Nat Commun*, 2014; 5: 3867.

Meli G, Visintin M, Cannistraci I, Cattaneo A. Direct *in vivo* intracellular selection of conformation-sensitive antibody domains targeting Alzheimer's amyloid-beta oligomers. *J Mol Biol*, 2009; 387(3): 584-606.

Ming GL, Song H. Adult neurogenesis in the mammalian brain: significant answers and significant questions. Neuron, 2011; 70:687-702.

Mu Y, Gage FH. Adult hippocampal neurogenesis and its role in Alzheimer's disease. *Mol Neurodegener*, 2011; 6:85.

Ono K. Alzheimer's disease as oligomeropathy. *Neurochem Int*, 2017.

Perez JL, Carrero I, Gonzalo P, Arevalo-Serrano J, Sanz-Anquela JM, Ortega J, Rodriguez M, Gonzalo-Ruiz A. Soluble oligomeric forms of beta-amyloid (Abeta) peptide stimulate Abeta production via astrogliosis in the rat brain. *Exp Neurol*, 2010; 223(2): 410-421.

Puzzo D, Lee L, Palmeri A, Calabrese G, Arancio O. Behavioral assays with mouse models of Alzheimer's disease: Practical considerations and guidelines. *Biochem Pharmacol*, 2014; 88:450-467.

Rodriguez JJ, Olabarria M, Chvatal A, Verkhratsky A. Astroglia in dementia and Alzheimer's disease. *Cell Death Differ*, 2009; 16(3): 378-385.

Ruan L, Lau BW, Wang J, Huang L, Zhuge Q, Wang B, Jin K, So KF. Neurogenesis in neurological and psychiatric diseases and brain injury: From bench to bedside. *Prog Neurobiol*, 2014; 115C:116-137.

Selkoe DJ. Soluble oligomers of the amyloid beta-protein impair synaptic plasticity and behavior. *Behav Brain Res*, 2008; 192:106-13.

Sotthibundhu A, Li QX, Thangnipon W, Coulson EJ. Abeta(1-42) stimulates adult SVZ neurogenesis through the p75 neurotrophin receptor. *Neurobiol Aging*, 2009; 30:1975-85.

Spalding KL, Bergmann O, Alkass K, Bernard S, Salehpour M, Huttner HB, Boström E, Westerlund I, Vial C, Buchholz BA, Possnert G, Mash DC, Druid H, Frisén J. Dynamics of hippocampal neurogenesis in adult humans. *Cell*, 2013; 153:1219-27.

Tanzi RE, Bertram L. Twenty years of the Alzheimer’s disease amyloid hypothesis: a genetic perspective. *Cell*, 2005; 120:545–55.

Thal DR, Sassin I, Schultz C, Haass C, Braak E, Braak H. Fleecy amyloid deposits in the internal layers of the human entorhinal cortex are comprised of N-terminal truncated

fragments of Abeta. *J Neuropathol Exp Neurol*., 1999;58(2):210-6.

Tsushima H, Emanuele M, Polenghi A, Esposito A, Vassalli M, Barberis A, Difato F, Chieregatti E. HDAC6 and RhoA are novel players in Abeta-driven disruption of neuronal polarity. *Nat Commun*, 2015; 6: 7781.

Unger MS, Marschallinger J, Kaindl J, Hofling C, Rossner S, Heneka MT, Van Der Linden A, Aigner L. Early Changes in Hippocampal Neurogenesis in Transgenic Mouse Models for Alzheimer's Disease. *Mol Neurobiol*, 2016; 53(8): 5796-5806.

Vescovi AL, Galli R, Gritti A. Clonal analyses and cryopreservation of neural stem cell cultures. *Methods Mol Biol*, 2002; 198:115-23.

Vukovic J, Blackmore DG, Jhaveri D, Bartlett PF. Activation of neural precursors in the adult neurogenic niches. *Neurochem Int*, 2011; 59:341-6.

Waldau B, Shetty AK. Behavior of neural stem cells in the Alzheimer brain. *Cell Mol Life Sci*, 2008; 65:2372-84.

Walker FO. Huntington's disease. *Lancet*, 2007; 369:218-28.

Wang R, Dineley KT, Sweatt JD, Zheng H. Presenilin 1 familial Alzheimer's disease mutation leads to defective associative learning and impaired adult neurogenesis. *Neuroscience*, 2004; 126(2): 305-312.

Wen PH, Hof PR, Chen X, Gluck K, Austin G, Younkin SG, Younkin LH, DeGasperi R, Gama Sosa MA, Robakis NK, Haroutunian V, Elder GA. The presenilin-1 familial Alzheimer disease mutant P117L impairs neurogenesis in the hippocampus of adult mice. *Exp Neurol*, 2004; 188(2): 224-237.

Winner B, Kohl Z, Gage FH.Neurodegenerative disease and adult neurogenesis. *Eur J Neurosci*, 2011; 33:1139-51.

Wyss-Coray T, Loike JD, Brionne TC, Lu E, Anankov R, Yan F, Silverstein SC, Husemann J. Adult mouse astrocytes degrade amyloid-beta *in vitro* and in situ. *Nat Med*, 2003;9(4):453-7.

Zhao C, Deng W, Gage FH. Mechanisms and functional implications of adult neurogenesis. *Cell*, 2008; 132:645-60.

Zhao M, Momma S, Delfani K, Carlen M, Cassidy RM, Johansson CB, Brismar H, Shupliakov O, Frisen J, Janson AM Evidence for neurogenesis in the adult mammalian substantia nigra. *Proc Natl Acad Sci USA*, 2003; 100:7925–7930.

Ziabreva I, Perry E, Perry R, Minger SL, Ekonomou A, Przyborski S, Ballard C. Altered neurogenesis in Alzheimer's disease. *J Psychosom Re*, 2006; 61(3): 311-316.

Ziemka-Nałęcz M, Zalewska T. Endogenous neurogenesis induced by ischemic brain injury or neurodegenerative diseases in adults. *Acta Neurobiol Exp (Wars)*, 2012; 72:309-24.

alzforum.org

sigmaaldrich.com

8. Materials and methods

8.1 Brain Dissection and Tissue Processing

All experiments with transgenic and control mice were conducted according to national and international laws for laboratory animal welfare and experimentation (EEC council directive 86/609, OJ L 358, 12 December 1987; Dlgs 116/92). Prior to brain dissection, adult mice were anesthetized with about 1 ml of 2,2,2-tribromethanol (Sigma-Aldrich, St. Louis, MO, http://www.sigmaaldrich.com) and intracardially perfused with 4% paraformaldehyde (PFA). The whole brain was therefore extracted and the fixation continued in 4% PFA overnight at 4°C. After cryoprotection in 30% sucrose, brains were cryosectioned at 40 μm of thickness, and slices encompassing the SVZ and the olfactory bulbs (OB) were analyzed by immunohistochemistry.

8.2 *In Vivo* Bromodeoxyuridine Labeling

Bromodeoxyuridine (BrdU; Sigma-Aldrich, St. Louis, MO, http://www.sigmaaldrich.com, B9285) was administered to Tg2576 and control adult mice (1.5-2-month-old) at 100 mg/kg by daily intraperitoneal injections for 5 days. Animals were then sacrificed either 2 (for SVZ) or 21 days (for OB) after the last injection, and brains were collected and processed as described before.

8.3 Neural Stem Cell Cultures

NSCs cultures were performed as described in Scardigli *et al*., 2014. 1.5-2-montholdmice (wild-type or Tg2576) were anesthetized as described before and killed by decapitation. After one week in culture, primary neurospheres were counted and their size were calculated. The size of neurospheres was expressed as their diameter in phase contrast pictures. Brightness and contrast images of live neurospheres were taken at a Nikon Eclipse Inverted TE 2000-E microscope, using NIS Elements 3.0 software. After, primary neurospheres were subcultured by mechanical dissociation into single cells every 4th day.

8.4 Proliferation Curve and Neural Stem Cell Differentiation

5 X 10^3 viable cells (2,5 X 10^3 /cm2 cell density) were initially plated in a T24 multiwell in growing medium. After 7 days *in vitro*, the total number of viable cells was counted by Trypan blue exclusion, and all cells were replated under the same cell density. This procedure was repeated for at least four subculture passages, in order to provide the statistical mean of the proliferation index of Tg2576 versus wild-type progenitors.

To assess for differentiation, neurospheres were dissociated into single cells and transferred onto matrigel-coated glass coverslips (12 mm diameter) in differentiating medium (growth medium without EGF and FGF) at 5 X 10^4 cells density. Five days after plating, cultures were fixed in 4% PFA at RT for 10 minutes and processed for immunocytochemistry.

8.5 hiPSCs Cultures

HiPSCs were used under the responsibility of Dr. Giovanni Meli (Group Leader, EBRI), exclusive recipient of iPSCs CiRA clones obtained from Dr. H. Inoue and Dr. K Okita (CiRA, Kyoto University), according with two active Material Transfer Agreements (MTAs). HiPSCs cultures were cultured on MEFs feeder layer in Human IPS Medium consisting of DMEM/F-12 (ThermoFischer Scientific, Waltham, MA, http://www.thermofisher.com, 10565-018) supplemented with 20% Knockout serum replacement (KSR, ThermoFischer Scientific, Waltham, MA, http://www.thermofisher.com, 10828028), P/S 100X (ThermoFischer Scientific, Waltham, MA, http://www.thermofisher.com, 15140-122), L-Glutamine 100X (ThermoFischer Scientific, Waltham, MA, http://www.thermofisher.com, 25030081), 50mM 2-Mercaptoethanol (ThermoFischer Scientific, Waltham, MA, http://www.thermofisher.com, 31350-010), Non-essential amino acids solution (MEM NEAA 100X, ThermoFischer Scientific, Waltham, MA, http://www.thermofisher.com, 11140-050) and human recombinant basic fibroblast growth factors(bFGF , Tebu-bio, Magenta, Italy, https://www.tebu-bio.com, 167100-18B-B) 10µg/mL.

After 7-10 days hiPSCs colonies should have grown to appropriate size for the expansion. The day before hiPSCs passaging, a feeders cells were prepared, plating 200.000 inactivated MEFs for each well of 0.1% gelatin solution (Sigma-Aldrich, St. Louis, MO, http://www.sigmaaldrich.com, G1890)-coated 6-well plate in MEFs medium consisting in Knockout DMEM (ThermoFischer Scientific, Waltham, MA, http://www.thermofisher.com, 10829018) supplemented with 7% FBS (ThermoFischer Scientific, Waltham, MA, http://www.thermofisher.com, 16000044), P/S 100X (ThermoFischer Scientific, Waltham, MA, http://www.thermofisher.com, 15140-122), L-Glutamine 100X (ThermoFischer Scientific, Waltham, MA, http://www.thermofisher.com, 25030081). Once the colonies are cleaned (using an insulin-needle under a magnifying glass to remove differentiated cells from the colonies) were divided in smaller pieces drawing a grid on colonies using an insulin-needle and were picked with a 1000µl micropipette, transferring the colony fragments into 6-well plate. After 48 hours, the medium was changed every day.

8.6 hiPSCs Differentiation

hiPSCs cultures were differentiated into primitive neural stem cells (pNSCs) as described in Yan *et al*., 2013. Briefly, hiPSCs cultured on MEFs feeder layer were split as cell clumps into six-well plates at density of $2.5X10^4$ cells per cm^2. 24 hours after splitting culture medium was switched to Gibco PSC Neural Induction Medium, containing Neurobasal medium and Gibco PSC neural induction supplement (ThermoFischer Scientific, Waltham, MA, http://www.thermofisher.com, A1647801). Neural induction medium was change every day from day 0 to day 7 of neural induction. At day 7 of neural induction, pNSCs were dissociated with Accutase (ThermoFischer Scientific, Waltham, MA, http://www.thermofisher.com, A1110501) and plated on Geltrex-coated dished at density of 10^5 cells per cm^2 in an NSC expansion medium, containing 50% Neurobasal medium (ThermoFischer Scientific, Waltham, MA, http://www.thermofisher.com, A1647801), 50% Advanced

DMEM/F12 (ThermoFischer Scientific, Waltham, MA, http://www.thermofisher.com, 12634010) and neural induction supplement. NSC expansion medium was changed every other day until NSCs reached confluence. For pNSCs before passage 4, 5µM ROCK inhibitor Y27632 (Sigma-Aldrich, St. Louis, MO, http://www.sigmaaldrich.com, SCM075) was added to NSC expansion medium at the time of NSC plating.

pNSCs cultures were differentiated into both neural lineage and glial lineage as described in Yan *et al*., 2013. In particular, for neuron differentiation, Accutase-dissociated pNSCs at passage 6 were plated onto laminin (10 µg/ml; ThermoFischer Scientific, Waltham, MA, http://www.thermofisher.com, 23017015)-coated glass coverslips (12 mm diameter) at a density of $5X10^4$ cells per cm^2 in a neuronal differentiation medium consisting of Neurobasal medium (ThermoFischer Scientific, Waltham, MA, http://www.thermofisher.com, A1647801), B-27 (ThermoFischer Scientific, Waltham, MA, http://www.thermofisher.com, 12587-010), GlutaMAX (ThermoFischer Scientific, Waltham, MA, http://www.thermofisher.com, 35050061), nonessential animal acids (MEM NEAA 100X, ThermoFischer Scientific, Waltham, MA, http://www.thermofisher.com, 11140-050), 20 ng/ml brain-derived neurotrophic factor (BDNF, Peprotech, Rocky Hill, NJ, https://www.peprotech.com, 450-02), 20 ng/ml glial cell-derived neurotrophic factor (GDNF, Peprotech, Rocky Hill, NJ, https://www.peprotech.com, 450-10), and 200 µM L-ascorbic acid (Sigma-Aldrich, St. Louis, MO, http://www.sigmaaldrich.com, A4034-100G) for 14 days, and the culture medium was changed every 2–3 days. Instead, for astrocytes differentiation, dissociated pNSCs at passage 6 were plated onto Geltrex-coated 24-well plate at a density of $5\ X10^4$ cells per cm^2 in an astrocyte differentiation medium, containing DMEM (ThermoFischer Scientific, Waltham, MA, http://www.thermofisher.com, 11965-092) supplemented with N2 and 1% fetal bovine serum (ThermoFischer Scientific, Waltham, MA, http://www.thermofisher.com, 10082147) for 21 days. Confluent cultures were passaged at a ratio of 1:4, and medium was changed every 2–3 days.

8.7 ScFvA13 and human Aβ oligomers Treatment on Cell Cultures

Cells in proliferative condition were treated with 0.2nM ScFvA13 (see Meli *et al*., 2009 for details) for 5 days every single day, while differentiated cells were treated for one week in expansion condition and during the differentiation time (five days) every single day. The treatment with 50nM or 10nM human Aβ oligomers, instead, was administered to WT progenitors every other day.

8.8 Immunocytochemistry on Brain Sections and Neurospheres

Immunohistochemistry of SVZ and OB was performed on 40-µm serial free-floating sections. To improve the efficiency of BrdU detection, the sections were treated as described in Scardigli *et al*., 2014. Upon fixation, sections or cells were permeabilized in blocking solution (0.3% or 0.1% Triton X-100, respectively, in PBS, 3% or 10% normal donkey serum and normal goat serum, respectively) and then incubated with the antibody of interests, described below. The total number of cells in each field was determined by counterstaining cell nuclei with 4,6-diamidine-2-phenylindole dihydrochloride (DAPI; Sigma-Aldrich, St. Louis, MO, http://www.sigmaaldrich.com; 50 mg/ml in PBS for 15 minutes at RT).

Immunostained sections and cells were mounted in Aqua-Poly/Mount (Polysciences, Inc., Warrington, PA, http://www.polysciences.com) and analyzed at fluorescent or confocal microscopy, using a Nikon Eclipse 90i microscope (Nikon) or a TCS SP5 microscope (Leica Microsystem). Z-stacks images were captured at 1 mm intervals with a 340 or 360 objectives and a pinhole of 1.0 Airy unit. Analyses were performed in sequential scanning mode to rule out cross-bleeding between channels. Fluorescence intensity quantification was performed with ImageJ software.

Primary antibody used: rat monoclonal anti-BrdU (BioRad, Berkeley, CA, USA, http://www.bio-rad.com, MCA2060, 1:400), rabbit polyclonal anti-Ki67 (Abcam, Cambridge, UK, http://www.abcam.com, ab16667, 1:200), rabbit polyclonal anti-activated Caspase-3 (cleaved caspase-3,

Cell Signalling Technology, 9664, 1:1,000), 12F4 (Biolegend, San Diego, CA, http://www.biolegend.com, SIG-39142, 1:250), mouse monoclonal anti-NeuN (Merck Millipore, Germany; MAB377, 1:500), rabbit polyclonal anti-glial fibrillary acid protein (DakoCytomation, Denmark, http://www.dako.com, Z0334, 1:500), goat anti-glial fibrillary acid protein (Santa Cruz Biotechnology, Dallas, TX, USA, http://www.scbt.it, sc-6170, 1:300) goat anti-Sox2 (Santa Cruz Biotechnology, Dallas, TX, USA, http://www.scbt.it, sc-17320, 1:300), goat anti-doublecortin (Santa Cruz Biotechnology, Dallas, TX, USA, http://www.scbt.it, sc-8066, 1.300), rabbit anti-calretinin (Swant, Bellinzona, Switzerland, www.swant.com, 7699/4, 1:300), goat anti-calbindin (Santa Cruz Biotechnology, Dallas, TX, USA, http://www.scbt.it, sc-7691, 1:1,000), mouse monoclonal anti-Neuronal class III β-Tubulin (Covance, Princeton, NJ, USA, http://www.covance.com, MMS-435P, 1:250), chicken anti-Neuronal class III β-Tubulin (Abcam, Cambridge, UK, http://www.abcam.com, ab41489, 1:500), rabbit anti-β-Amyloid D54D2 (Cell Signaling Technology, Danvers, MA, USA, http://www.cellsignal.com, 8243, 1:200), rabbit monoclonal anti- Green Fluorescent Protein JL-8 (Clontech, CA, USA, http://www.clontech.com, 632381, 1:500), mouse monoclonal anti-Acetylated Tubulin (Sigma-Aldrich, St. Louis, MO, http://www.sigmaaldrich.com, T7451, 1:500), rat anti-tubulin alpha (BioRad, Berkeley, CA, USA, http://www.bio-rad.com, MCA77G, 1:200), mouse anti-Tau1 (Merck Millipore, Germany, http://www.millipore.com, MAB3420, 1:200), mouse anti- Phospho-PHF-tau pSer202+Thr205 AT8 (ThermoFisher Scientific, Waltham, MA, USA, http://www.thermofisher.com, MN1020, 1:200), rabbit anti-calnexin (Sigma-Aldrich, St. Louis, MO, http://www.sigmaaldrich.com, C4731, 1:2,500), rabbit polyclonal anti-human calreticulin (CusAb, MD, USA. http://www.cusabio.com, CSB-PA07864A0RB, 1: 200), anti-V5 Tag (ThermoFischer Scientific, Waltham, MA, http://www.thermofisher.com, R960-25, 1:1,000).

Secondary antibodies used: (ThermoFisher Scientific, Waltham, MA, USA, http://www.thermofisher.com): donkey-anti rabbit antiserum conjugated to Alexa 488 or to Alexa594, or to Alexa

647, donkey-anti mouse antiserum conjugated to Alexa 488 or to Alexa 594, or to Alexa 555 or to Alexa 647, goat anti-rat conjugated to Alexa 594, donkey anti-goat antiserum conjugated to Alexa 488 or to Alexa 594, or to Alexa 555, or to Alexa 647, donkey anti-chicken antiserum conjugated to Alexa 647.

8.9 Quantification of Cell Numbers

Stereological analysis of the number of cells was performed on series of 40-μm free-floating coronal sections comprising the entire SZV or OB, which were analyzed by confocal microscopy to count cells expressing BrdU, counting three regions per section (top, central, and bottom). To obtain the average number of SVZ or OB cells per square millimeter, the number of positive cells for each SVZ and OB section was multiplied by the total number of sections encompassing the entire structure. Three animals per group (n=3) were analyzed.

Statistical analysis was performed by unpaired Student's t test, and all experiments were expressed as mean +SEM.

To quantify the number of differentiated cells, the number of Tuj1 and glial fibrillary acid protein (GFAP) immunoreactive cells was counted in at least 10 non-overlapping fields in each sample, for a total of >1,000 cells per sample. The total number of cells in each field was determined by counterstaining cell nuclei with DAPI (Sigma-Aldrich, St. Louis, MO, http://www.sigmaaldrich.com, D9542, 50 mg/ml in PBS for 15 minutes at RT). The average percentage of differentiated cells for each sample was then calculated by dividing the number of Tuj1 and GFAP positive cells by the total number of cells for each field. Data are the mean +SEM of three independent cultures, constituted by pool of two or three animals (n=6), three independent experiments for each culture. Statistical analysis was performed by unpaired Student's t test.

To quantify neuritic processes, the length of Tuj1-labeled filaments was measured in 7 non-overlapping fields through semi-automatic filament count using IMARIS software. Filament seed points were manually added by an experimenter blind to group samples. Total filament length in each field was divided by the number of DAPI-positive cells and expressed as

average density of neurite ramification per cell. Statistical analysis was performed by one-way ANOVA.

8.10 Lentiviral Vectors Preparation and Neurospheres Infection

The ScFvA13KDEL gene was cut by scFv-intrabody vectors (Meli *et al*, 2014) and insert in the pRRL-CMV-PGK-GFP-WPRE (TWEEN) vectors in the XbaI site. This bicistronic vector allows the simultaneous expression of the GFP and ScFvA13KDEL. The lentivirus vectors were prepared by the transient transfection of 293T cells using the calcium phosphate precipitation method. In particular, 293T cells were transfected with TWEEN vectors together with pMDL/pRRE, pMDG2.G and pRSV-Rev overnight. After that the medium of 293T cells was changed. The day after and on day 2 of change medium, 293T cells medium, containing lentivirus vectors, was collected, pelleted, filtered and ultracentrifugated at 2600rpm for 2 hours at 4°C. The resulting pellet was risuspended in 200 µl of HBSS, aliquotated and stored at -80°C for the following experiments. The titer of lentivirus vectors was 1.7×10^7 IFU/µl and was measured by p24-test ELISA kit. $1 \text{ X } 10^5$ viable cells were plated in a T24 multiwell in growing medium and infected with 5µl of TWEEN-A13KDEL lentiviral vector for 8 hours. The day after neurospheres medium was change and 48 hours the infection was controlled by the GFP expression at fluorescence microscope.

Instead, in the inducible lentiviral vector, pTRE_A13KDEL, ScFvA13KDEL gene was cloned in an inducible lentivirus vector (Cattaneo and Marchetti group, unpublished data).

8.11 Sample preparation for biochemical analysis

For conditioned medium (CM) preparation, cells were grown to ~90% confluence, CM was collected and cleared of cell debris by centrifugation at 200g for 10 min. The Ponceau S staining of nitrocellulose membrane before western blot (WB) and dot blot (DB), which detect the total proteins, was used as normalization of WB lanes loading an DB spots (see also Supplementary Information). In order to improve the detection of Aβ

Oligomers (AβOs, without immunoprecipitation steps), we performed a procedure of concentration of the CM by centrifugation steps, as described in Meli *et al*., 2014, and we established that a 1X and 3X concentration allows a sensitive discrimination of AβOs (in comparative analyses of WT and Tg2576 CM). Cell lysates were done in Tris-HCl pH8 50 mM, NaCl 150mM, NP40 1% with the addition of cocktail of proteases and phosphatases inhibitors (Roche). The lysates were centrifuged at 13,000rpm for 20 min. The supernatant was collected and the concentration of total proteins was determined by BCA assay. In this case, the β-actin staining was used as normalization of WB lanes loading.

8.12 Western Blot Assay for Aβ

Samples (CM or cell lysates) were diluted in NuPAGE™ LDS sample buffer (4X, ThermoFisher Scientific, Waltham, MA, http://www.thermofisher.com, NP0007) and 10X DTT solution 1M (Applichem, Germany, http://www.applichem.com, A3668,0050), boiled 10 min, loaded in precasted NuPAGE™ Novex™ 10% Bis-Tris Midi Protein Gels (ThermoFisher Scientific, Waltham, MA, http://www.thermofisher.com, WG1201A), running in NuPAGE MES SDS running buffer (ThermoFisher Scientific, Waltham, MA, http://www.thermofisher.com, NP0002). The semidry blot was then done onto nitrocellulose membrane filters, 0.22 mm (GE Healthcare, Buckinghamshire, UK, http://http://www.gehealthcare.com, 10600001). The membrane filter was boiled in PBS to increase the detection of low MW bands. After the incubation with the blocking solution (TBS 0.05% tween, 5% dry milk), antibodies were used in TBS 0.05% tween, 2,5% dry milk and ECL (GE Healthcare, Buckinghamshire, UK, http://http://www.gehealthcare.com, RPN2209) chemiluminescent detection was performed.

Antibodies used: Anti-Aβ/WO2 (Merck Millipore, Germany, http://www.millipore.com, MABN10, 1:1,000), anti-APP C-terminal fragment (Sigma-Aldrich, St. Louis, MO, http://www.sigmaaldrich.com, A8717, 1:3,000), anti-APP N-terminal 22C11 (Merck Millipore, Germany, http://www.millipore.com, MAB348SP, 1:1,000), anti-V5 Tag (ThermoFischer Scientific, Waltham, MA, http://www.thermofisher.com, R960-25, 1:1,000), anti-b-Actin (Sigma-Aldrich, St. Louis, MO, http://www.sigmaaldrich.com, A2228, 1:5000), anti-mouse-HRP (Jackson ImunnoReasearch, West Baltimore Pike, West Grove, PA, https://www.jacksonimmuno.com, 715-035-151, 1:4,000), anti-rabbit-HRP (Jackson ImmunoResearch, 711-035-152, 1:4,000).

8.13 Dot Blot analysis

Concentrated and not-concentrated CM and cellular samples were spotted onto nitrocellulose membrane filters 0.22 mm (GE Healthcare, Buckinghamshire, UK, http://www.gehealthcare.com, 10600001). After incubation with the blocking solution (TBS 0.05%, or 0.01% tween, 10% dry milk), antibodies were used in TBS 0.05% tween, 5% dry milk or TBS 0.01% tween, 5% dry milk only for anti-oligomer A11 (Merck Millipore, Germany, http://www.millipore.com, AB9234, 1:500), and ECL (GE Healthcare, Buckinghamshire, UK, http://www.gehealthcare.com, RPN2209) chemiluminescent detection was performed. Anti-AβOs scFvA13 (3.5 $mgml^{-1}$) was used as described in Meli *et al*., 2014. Serial dilution curves of cellular samples were preliminarily tested to obtain non-saturating condition of immunodetection and samples were loaded at 1μg/μl, whereas CM were spotted at 1X and 3X concentration.

Antibodies used: anti-oligomer A11 (Merck Millipore, Germany, http://www.millipore.com, AB9234, 1:500), scFvA13, anti-Amyloid Fibrils OC (Merck Millipore, Germany, http://www.millipore.com, AB2286, 1:1,000), Anti-Abeta42 (Synaptic Sistems, Germany, https://www.sysy.com, 218721, 1:1,000), anti-His tag (Merck Millipore, Germany, http://www.millipore.com, 05949, 1:2,000), anti-mouse-HRP (Jackson ImunnoReasearch, West Baltimore Pike, West Grove,

PA, https://www.jacksonimmuno.com, 715-035-151, 1:4,000), anti-rabbit-HRP (Jackson ImmunoResearch, West Baltimore Pike, West Grove, PA, https://www.jacksonimmuno.com, 711-035-152, 1:4,000).

8.14 Sample preparation and Western blot analysis for cytoskeleton

Total proteins were extracted by scraping the cells in ice-cold RIPA buffer (50 mM Tris-HCl pH 8, 150 mM NaCl, 1% NP40, 0,1% SDS, 5% sodium deoxicholate plus proteases inhibitor cocktail (Sigma-Aldrich, St. Louis, MO, http://www.sigmaaldrich.com, P8340) and phosphatase inhibitor cocktail (Sigma-Aldrich, St. Louis, MO, http://www.sigmaaldrich.com, P5726/P2850) and centrifuged at 4 °C for 20 min at 13000 rpm. The supernatant was then collected and the amount of total protein was determined by Bradford assay (Protein Assay Dye Reagent Concentrate, BioRad, Berkeley, CA, USA, http://www.bio-rad.com). Equal amounts of protein were separated by 10 and 12% SDS–PAGE and transferred to nitrocellulose membrane filters 0.45µm (GE Healthcare, Buckinghamshire, UK, http://http://www.gehealthcare.com, 10600002). The filters were blocked in TBS-T containing 5% non-fat dried milk for 1h at room temperature or overnight at 4°C. Proteins were visualized using appropriate primary antibodies. All primary antibodies were diluted in TBS-T and incubated with the nitrocellulose blot overnight at 4°C. Incubation with secondary peroxidase coupled anti-mouse, anti-rabbit or anti-goat antibodies was performed by using the ECL system (SuperSignal West Pico, ThermoFisher Scientific, Waltham, MA, http://www.thermofisher.com, 34080; ECL Prime, GE Healthcare, Buckinghamshire, UK, http://http://www.gehealthcare.com, RPN2232). Protein loading was monitored by normalization to GAPDH level . Blots were scanned and quantitative densitometric analysis was performed by using ImageJ (http://imagej.nih.gov/ij/).

Antibodies used: mouse acetylated α Tubulin 6-11B-1 (Santa Cruz Biotechnology, Dallas, TX, USA, http://www.scbt.it, sc-23950, 1:1500); rat anti tubulin alpha mouse

(BioRad, Berkeley, CA, USA, http://www.bio-rad.com, MCA77G, 1:1000); mouse GAPDH antibody 6C5 (Santa Cruz Biotechnology, Dallas, TX, USA, http://www.scbt.it, sc-32233, 1:4000); Tau-1, Ser-195/Ser-198 epitopes, dephosphorylation-dependent state (Merck Millipore, Germany, http://www.millipore.com, MAB3420, 1:1000); AT8, pSer202/pThr20 epitopes, phosphorylation-dependent state (ThermoFisher Scientific, Waltham, MA, http://www.thermofisher.com, MN1020, 1:500); anti-mouse IgG (whole molecule)-Peroxidase antibody (Sigma-Aldrich, St. Louis, MO, http://www.sigmaaldrich.com, A4416, 1:10000).
Data presented are representative of at least three independent experiments and were expressed as mean ± SEM. Statistical analysis of all the experiments in this study were performed by GraphPad Prism (GraphPadSoftware) , using appropriate test, i.e. paired or unpaired Student's t-test.

8.15 Stereotaxic surgery

Mice were anesthetized with 50 mg/kg solution of Zoletil (100 mg/ml) and Rompun (20 mg/ml) and mounted on stereotaxic apparatus. Injecting cannulae were inserted into the sub-ventricular zone, SVZ (coordinates relative to bregma: +0.6 anteroposterior, +1 lateral and -2.7 ventral). Injections were performed using a 10μl hamilton syringe connected to a gauge injector.
Mice were injected unilaterally with 1μl of scFv_A13K ($1.7X10^7$ IFU/μl), in one hemisphere while the opposite hemisphere was not injected and used as internal control. Mice were killed 10 days after the injections through perfusion in 4% PAF.